# Atomically Dispersed Supported Metal Catalysts

Maria Flytzani-Stephanopoulos[1] and Bruce C. Gates[2]

[1]Department of Chemical and Biological Engineering, Tufts University, Medford, Massachusetts 02155; email: maria.flytzani-stephanopoulos@tufts.edu

[2]Department of Chemical Engineering and Materials Science, University of California, Davis, California 95616



Annu. Rev. Chem. Biomol. Eng. 2012. 3:545–74

First published online as a Review in Advance on April 24, 2012

The *Annual Review of Chemical and Biomolecular Engineering* is online at chembioeng.annualreviews.org

This article's doi: 10.1146/annurev-chembioeng-062011-080939



1947-5438/12/0715-0545$20.00

## Keywords

noble metal cations, gold, zeolites, oxide supports, mononuclear ensembles, CO oxidation, water-gas shift reaction, ethylene hydrogenation

## Abstract

Our aim in this review is to assess key recent findings that point to atomically dispersed noble metals as catalytic sites on solid supports, which may be viewed as ligands bonded to the metal. Both zeolites and open metal oxide supports are considered; the former offer the advantages of uniform, crystalline structures to facilitate fundamental understanding, and the latter offer numerous advantages in applications. The notion of strong interactions between metals and supports has resurfaced in the recent literature to explain how subnanometer clusters and even atoms of noble metals such as platinum and gold survive under often harsh reaction conditions on some supports, such as ceria and perovskites. Individual cations of platinum, palladium, rhodium, or other metals anchored to supports through M–O bonds can be formed on these supports in configurations that are stable and catalytically active for several reactions illustrated here, notably, oxidation and reduction. The development of effective synthesis methods and the identification of suitable stabilizers and promoters are expected to lead to the increasing application of atomically dispersed noble metal catalysts for practical processes characterized by efficient resource utilization and cost savings.

## INTRODUCTION: METAL CATALYSTS ATOMICALLY DISPERSED ON SUPPORTS

Many industrial catalysts consist of expensive metals dispersed on inexpensive high-area porous supports. When the dispersions are high, many of the metal atoms are present at a surface, accessible to reactants and available for catalysis. In the limit, the metals are atomically dispersed, constituting the emerging class of catalysts emphasized here. Industrial catalysts in this class are used for olefin polymerization, including single-site metallocenes (e.g., complexes of zirconium and of hafnium) and silica-supported complexes of chromium.

Atomically dispersed metal catalysts also include transition metal compounds (complexes) used in solution and stabilized by ligands. These compounds are mononuclear—each molecule or ion incorporates a single metal atom. Many industrial catalysts consist of complexes of transition metals, in particular noble (group 8) metals. The soluble catalysts that are industrially successful are often highly selective, consistent with the uniformity of the catalytic species (1). The uniformity facilitates structural elucidation and fundamental understanding. However, the soluble catalysts suffer from the technological disadvantages of expensive separation from products and corrosion.

To maintain the advantages of molecular catalysts in solution and minimize their disadvantages, researchers have prepared catalysts consisting of mononuclear transition metal complexes anchored to solid supports. Many of these are analogs of soluble catalysts, including numerous metal oxide– and organic polymer–supported catalysts for low-temperature reactions such as olefin hydrogenation, olefin hydroformylation, and methanol carbonylation (2–5).

Supported metal complex catalysts have found few industrial applications with liquid-phase reactants because the metals are leached. When a supported metal complex catalyst is used with gas-phase reactants, however, leaching is prevented, and—if the catalyst is stable—it can be used at high temperatures. The stability challenge points to robust supports and stably anchored catalytic species.

Most supported metal catalysts consisting of clusters or particles of metal are characterized by the cluster or particle size and exposed metal surface area. As the size of the metal structure is reduced to subnanometer clusters and further to atoms/ions, its catalytic properties change. Interest in atomically dispersed catalytic sites focuses on methods for their synthesis and stabilization to maximize the efficiency of the precious metal use and minimize the cost (6).

The goal of reducing the amount of platinum-group metals in automotive catalytic converters has driven environmental catalysis research for three decades. Other major accomplishments are associated with the substantial replacement of platinum and rhodium with the less expensive palladium in automotive three-way catalysts (TWCs) (7) and diesel oxidation catalysts (8). Reducing the amount of platinum in electrocatalysts for polyelectrolyte membrane fuel cells is a long-standing challenge that limits the large-scale application of fuel cells. Much of the research in this area has focused on the (still largely unsuccessful) search for replacements for platinum and on the formation of platinum surface alloys on a cheaper metal backbone (9). These issues are also potentially crucial for noble metal catalysts that are currently under development for (*a*) production of biomass-derived fuels and chemicals (10–12), (*b*) new energy generation systems involving fuel processing catalysts (13), and (*c*) energy storage applications (14).

The atomically dispersed supported metal catalyst field is lively and growing, and much recent work focuses on noble metals. Here we review this field, emphasizing recent research and citing reviews to link to earlier work. Our review focuses on the most thoroughly characterized catalysts and is not comprehensive.

# MONONUCLEAR METAL COMPLEXES ON ZEOLITE SUPPORTS

## Motivation for Use of Zeolites as Supports

The motives for investigating atomically dispersed supported metals are to understand their structures and properties and to discover new catalysts. To address the first objective, researchers have prepared samples that are structurally uniform and characterizable. Because the support is an essential part of the catalytic species, it needs to be structurally uniform—hence crystalline. Thus, zeolites (crystalline aluminosilicates, materials with intracrystalline pores that have diameters typically on the order of 1 nm) have been widely investigated as supports; they are the focus of the first part of our review.

Zeolites are widely used as industrial catalysts and catalyst supports, in particular faujasites, zeolite Y, and zeolite X (with a unit cell formula being $Na_j[AlO_2]_j(SiO_2)_{192-j}\cdot zH_2O$). The zeolite structure consists of $SiO_4$ tetrahedra linked by shared oxygen atoms, and Al can replace as many as half of the Si atoms. Because the Al atoms bear charges of +3 and the Si atoms charges of +4, the aluminosilicate frame requires exchange cations for charge neutrality. The classes of zeolite-supported metal complex catalysts include (*a*) those in which mononuclear metal complexes are bonded to oxygen ions of the zeolite lattice (the zeolite is a ligand), (*b*) those in which the metal ions are part of the zeolite framework, (*c*) those with molecular metal complexes trapped in their pores, and (*d*) those in which the metal complexes are anchored to the support via organic tethers. The metals in class (*a*) usually incorporate ligands in addition to the zeolite, and they are molecular analogs. The metals in classes (*b*), (*c*), and (*d*) are outside the scope of this review.

Incorporation of a metal in an atomically dispersed form on a zeolite or oxide almost always implies that it is cationic, and thus not in the form most commonly encountered in supported metal catalysts. Single zerovalent noble metal atoms on supports are unstable and aggregate readily into metallic particles. They are outside the scope of this review.

## Synthesis

Supported mononuclear metal complexes can be formed by chemisorption of a reactive mononuclear metal complex precursor (usually an organometallic) from the gas or liquid phase onto the support. The syntheses are carried out with exclusion of air and water, which react with most organometallic compounds. Another preparation involves the chemisorption of a metal salt on a support or ion exchange followed by calcination (which gives ill-defined supported species), followed by reduction to form metal clusters or particles, followed by oxidation to form fragmented species that may be mononuclear (15–19). In regeneration of conventional supported metal catalysts (e.g., those used for naphtha reforming in gasoline manufacture), such a process is called redispersion. The oxidizing agent is commonly $O_2$ or $Cl_2$. Oxidation of supported metal particles does not always fragment them; instead, it may just oxidize the metal particle surface.

When supported metal complexes are formed on supports, surface oxygen atoms or hydroxyl groups of the support become ligands bonded to the metal. Because zeolites are often highly uniform, zeolite-supported species may be highly uniform—and essentially molecular in character. The uniformity of zeolite-supported species greatly facilitates structure determinations. But if the support is a metal oxide, then the surface species are nonuniform and more challenging to characterize, because oxide surfaces are intrinsically nonuniform and have chemistry that defect sites sometimes dominate.

It is often challenging to determine the ligands bonded to a supported metal complex. Besides the support, the ligands include other groups bonded to the metal, which are introduced during

catalyst preparation or subsequent treatments. Many reports of supported mononuclear metal species fail to address the nature of the ligands.

## Structural Characterization

Determination of the structures of supported metal complexes is typically based on spectroscopy, but high-resolution transmission electron microscopy (TEM), especially aberration-corrected scanning TEM (STEM), has recently emerged as an essential characterization tool. It is most effective when used in concert with spectroscopic methods and density functional theory (DFT). None of these techniques alone is ever sufficient. The characterizations are most informative when the supported species are uniform because the spectra are much more easily interpreted than when mixtures are present. The spectroscopic methods that have provided the most insight into the structures of supported metal complexes are IR, Raman, and X-ray absorption spectroscopies, including extended X-ray absorption fine structure (EXAFS) spectroscopy and X-ray absorption near edge structure (XANES) spectroscopy. The spectroscopic methods provide average structural information and are complemented strongly by the local structural information provided by STEM. A review of these techniques emphasizing catalysts of the type considered here was published in 2006 (20).

## Reactivity

Some of the most thoroughly characterized supported metal complexes are metal carbonyls, prepared, for example, by reaction of $Rh(CO)_2(acac)$ (acac is acetylacetonate) with a zeolite such as dealuminated zeolite HY, as acac ligands are removed from the rhodium and each Rh atom bonds to two zeolite oxygen atoms (21). $Rh(CO)_2$ can also be formed by adsorption of $[Rh(NH_3)_5Cl][OH]_2$ followed by reduction to give rhodium clusters, followed by oxidative fragmentation in CO (19).

The uniformity of the supported species is evidenced by the sharpness of the carbonyl IR bands. These site-isolated $Rh(CO)_2$ species are usually widely separated from each other. The samples are considered nearly ideal when the supported groups are site isolated and nearly uniform. Analogous species on oxide supports are characterized by broad carbonyl IR bands corresponding to the variety of surface anchoring sites.

The near-uniformity of structure of $Rh(CO)_2$ in dealuminated zeolite Y (**Figure 1**) implies that the bonding positions of the metal complex are nearly equivalent crystallographically (21). Thus, the carbonyl IR spectra provide information about the symmetry of the species and hence the support sites that are ligands in the rhodium complex. The spectra indicate a square-planar complex with rhodium formally in the +1 oxidation state, $Rh^I$, and with each Rh atom bonded to two zeolite oxygen atoms. EXAFS data confirm the presence of approximately two CO ligands and approximately two support oxygen atoms per Rh atom. Calculations at the level of DFT, with a fragment of the zeolite capped with hydrogen atoms used to represent the support, gave structure parameters for $Rh(CO)_2\{OAl\}_2$ (the braces denote the support surface) that are consistent with the spectra and the structural model of **Figure 1**. The only sites for $Rh(CO)_2$ bonding consistent with the results are the cation bonding sites shown in **Figure 1**, near the Al ions in the zeolite.

A family of supported rhodium complexes was formed from the supported $Rh(CO)_2$ by reaction with various gases as IR or EXAFS spectra were recorded, and the effluent gas was analyzed. The gases provided ligands to replace CO, including those derived from $H_2$, $D_2$, $N_2$, and ethylene (22). For example, two ethylene ligands replaced CO; each became $\pi$-bonded to the rhodium. $H_2$ reacted dissociatively to give hydride ligands. Even weakly bound ligands such as $N_2$ replace the strongly bound CO ligands when the gas is brought in contact with the solid sample in a

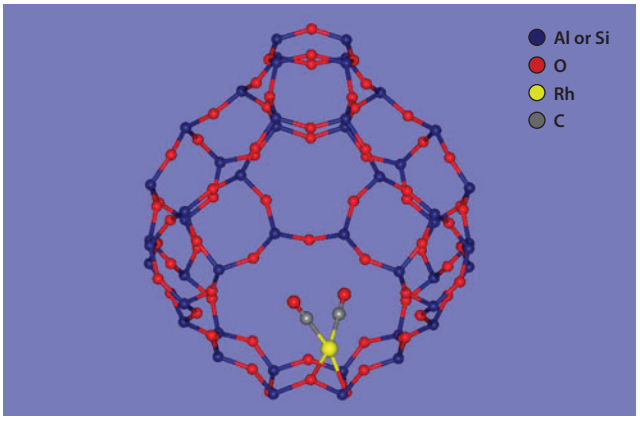


**Figure 1**

Structural model of $Rh(CO)_2$ supported by dealuminated Y zeolite as determined by spectroscopy and density functional theory calculations. The figure is not meant to represent bond angles accurately (21). Reproduced by permission of The Royal Society of Chemistry.

once-through flow reactor so that the dissociated CO ligands are swept away and no equilibrium limitation exists.

Similarly, complexes of other metals can be bonded to HY zeolite by reactions involving the following precursors: $Ir(C_2H_4)_2(acac)$ (23), $Ru(C_2H_4)_2(acac)_2$ (24), and $Au(CH_3)_2(acac)$ (25). These gave the following supported metal complexes: $Ir(C_2H_4)_2$, $Ru(C_2H_4)_2$, and $Au(CH_3)_2$. The reactions of the iridium complexes are similar to those of the rhodium complexes. $Ir(C_2H_4)_2$ species are also formed by reaction of $Ir(C_2H_4)_2(acac)$ with the zeolite HSSZ-53. STEM images showing isolated Ir atoms provide evidence of the site isolation and uniformity of the $Ir(C_2H_4)_2$ complexes (**Figure 2**) (26).

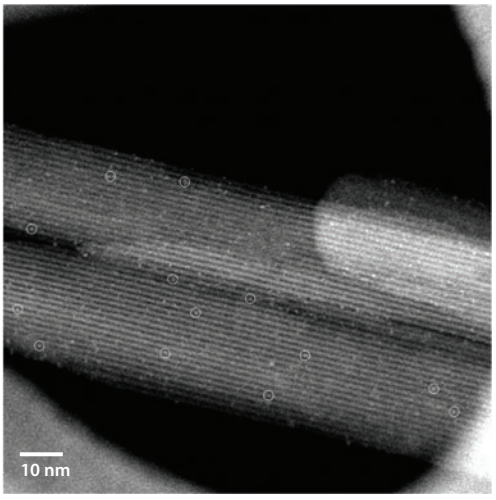


**Figure 2**

High-angle annular dark-field scanning transmission electron microscopy image of $Ir(C_2H_4)_2$ complexes on zeolite HSSZ-53. The bright features on the image are the site-isolated single Ir atoms; some are circled for emphasis (26).

The sample incorporating two π-bonded ethylene ligands per Rh atom is important (22) because its characterization by variable-temperature $^{13}C$ NMR spectroscopy provided the strongest evidence of the dynamic uniformity (and, by inference, the structural uniformity) of a zeolite-supported metal complex (27).

## Supports as Ligands

To probe the influence of supports as ligands, $Ru(C_2H_4)_2(acac)_2$ was used to form $Ru(C_2H_4)_2(acac)$ and $Ru(C_2H_4)_2$ complexes on the zeolites H-β, H-mordenite, HZSM-5, and H-SSZ-42 (28). Each reacted similarly with the precursor (except for transport limitations associated with the smaller-pored H-mordenite and HZSM-5). Each of the zeolite-supported ruthenium complexes was exposed to CO to form ruthenium dicarbonyls, the frequencies of which provide a sensitive indicator of the zeolites as ligands. The $\nu_{CO}$ frequencies show how the composition of the zeolite influences the bonding of the supported species. The frequency differences are small ($<10\ cm^{-1}$), but the effects are significant.

## Catalysis Illustrated for Complexes of Rhodium and of Iridium

Site-isolated $Rh(C_2H_4)_2$ and $Ir(C_2H_4)_2$ on MgO catalyze ethylene hydrogenation at atmospheric pressure and room temperature. This behavior is typical of supported group 8 metal complexes. A comparison of the catalytic performance of the MgO-supported iridium complex and the isostructural complex on HY zeolite demonstrates the influence of the support as a ligand. IR data demonstrate the electron-donor character of MgO and the electron-withdrawing character of the zeolite. The catalyst performance and spectra of the supported species demonstrate that the catalytic activity [measured as the turnover frequency (TOF)—the rate per Ir atom] is strongly dependent on the nature of the support. The zeolite-supported iridium complex has a catalytic activity more than 20 times that of the MgO-supported complex.

The high ethylene hydrogenation activity of the zeolite-supported iridium complexes matches the high activity of this catalyst for $H_2$ dissociation, which is measured by the catalytic activity for H–D exchange in reaction of $H_2 + D_2$. Accordingly, IR and EXAFS spectra of the zeolite-supported iridium complexes in $H_2$ at room temperature show that the ethylene ligands initially π-bonded to the Ir centers react readily to form ethyl groups. EXAFS and IR spectra of the catalyst in the working state indicate diethyl iridium, $Ir(C_2H_5)_2$, as a stable reaction intermediate. In contrast, on MgO, $Ir(C_2H_4)_2$ species are the stable intermediates. Thus, the support as a ligand affects the reactivity of the metal center, the nature of the stable reaction intermediates, and the rate-determining step in the catalytic reaction. The isolated iridium complexes on the zeolite were inferred to have a higher degree of coordinative unsaturation than those on MgO, a consequence of the electron-withdrawing character of the zeolite, which strongly reduces the electron density on the iridium. The role of the support as a ligand can be determined fundamentally when the metal species are essentially uniform and molecular in nature.

The catalytic properties of $Ir(C_2H_4)_2$ on MgO are similar to those of the isostructural rhodium complex on MgO. However, when the support was switched to HY zeolite, markedly different catalytic behavior was observed for $Rh(C_2H_4)_2$. The rhodium complex on the zeolite support is active for ethylene dimerization, even in the presence of $H_2$ (hydrogenation is a side reaction). Complexes of many transition metals catalyze C–C bond formation (and the production of polyolefins is an enormous technology), but these reactions have been carried out with complexes of early transition metals such as chromium, titanium, and zirconium. Late transition metals such as palladium and rhodium had been known to catalyze these reactions only in the presence of halides, which allow the metal to shuttle between oxidation states in the catalytic cycle. The unanticipated

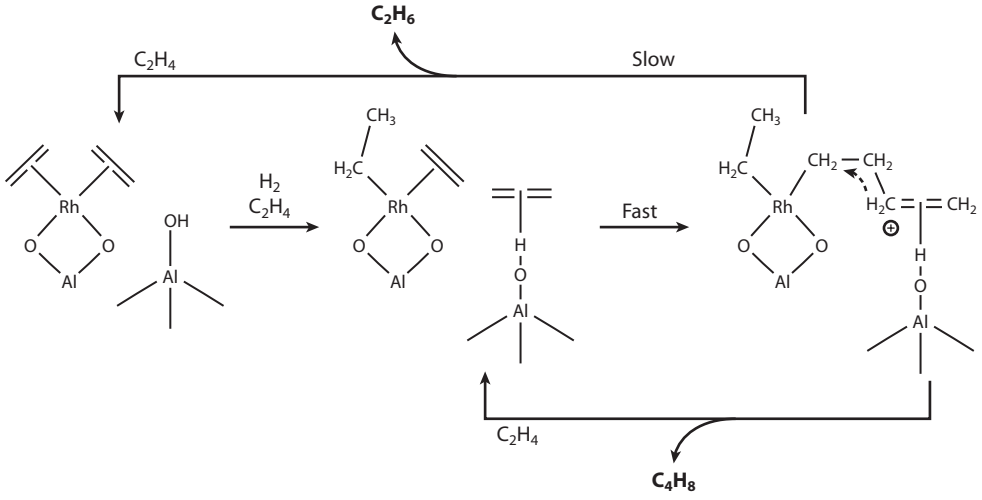


**Figure 3**

Simplified reaction mechanism for the conversion of ethylene on a zeolite-supported rhodium complex catalyst in the presence of $H_2$. The reaction intermediates are proposed on the basis of IR and extended X-ray absorption fine structure data, the results of $H_2/D_2$ exchange experiments, and catalyst performance data (29).

selectivity of the supported rhodium complex catalyst for C–C bond formation in the absence of halides shows how one can markedly alter the catalytic properties by changing the support.

Characterization of the dimerization catalyst in the working state by IR and EXAFS spectroscopies coupled with H/D exchange reaction experiments demonstrated that the catalysis involves cooperation between mononuclear rhodium complexes and Brønsted acid sites of the zeolite. $H_2$ promotes the dimerization reaction, and the ethyl species expected to be intermediates in the hydrogenation reaction were inferred not to be involved in the dimer formation. Spectra of the catalyst in reactive atmospheres and the results of experiments carried out with $D_2$ replacing $H_2$ indicate a cooperation between the metal complexes and Brønsted acid sites in the formation of C–C bonds (**Figure 3**) (29).

HY zeolite-supported $Rh(C_2H_4)_2$ is a precursor of a catalyst for acetylene trimerization to give benzene, and $^{13}C$ NMR spectra of the catalyst identified some stable reaction intermediates. DFT calculations agree well with the spectra and EXAFS structural data characterizing the observable species—and so further such calculations were applied to infer the full catalytic cycle (**Figure 4**). This example illustrates how much detail can be learned about zeolite-supported metal complex catalysts.

## Importance of Metal Clusters

Complexes of noble metals bonded to zeolite and oxide supports are readily converted into metal clusters and metallic particles; the metal in the latter is zerovalent. Reducing agents such as $H_2$ or heating of the sample can trigger the reduction/aggregation processes; autoreduction often occurs. It is challenging to distinguish mononuclear metal complexes from small metal clusters on supports, and when the complexes are present along with clusters or particles, it is challenging to identify the catalytic species, which may be a small minority. STEM has become important in the identification of such species in zeolites (31) and, as shown below, on oxides.

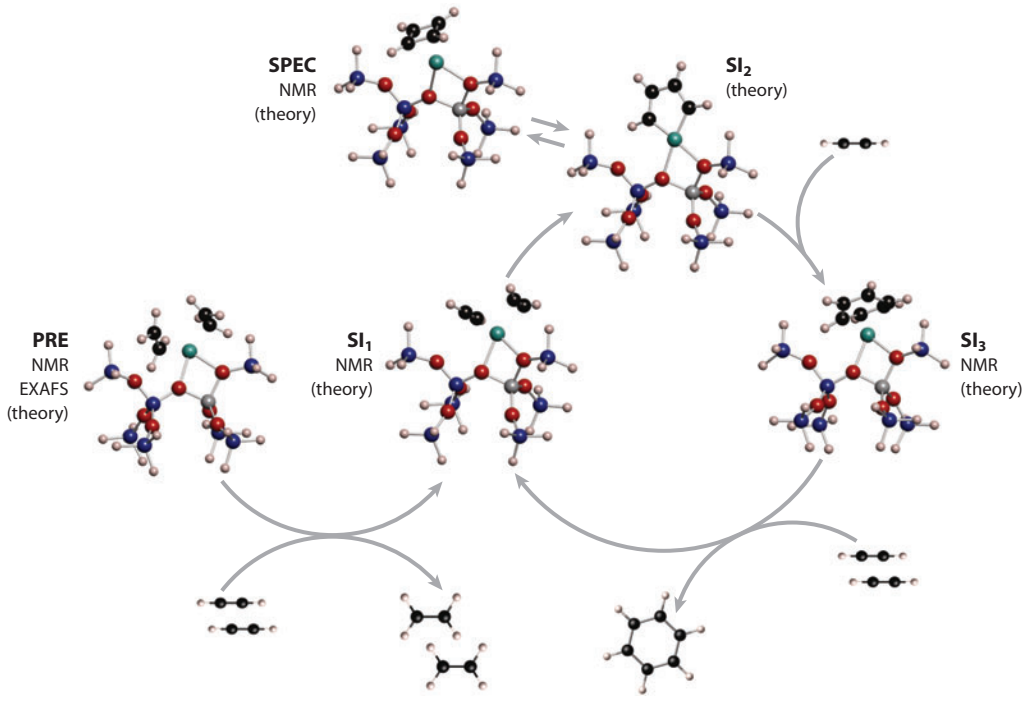


**Figure 4**

Catalytic cycle for trimerization of acetylene catalyzed by a mononuclear rhodium complex bonded to HY zeolite. The structures were determined by calculations at the level of density functional theory; the results agree within the expected errors with the results of extended X-ray absorption fine structure (EXAFS) and $^{13}C$ NMR spectroscopies. Abbreviations: PRE, catalyst precursor; SI, reaction intermediate; SPEC, spectator species. The zeolite was modeled in the calculations as a fragment of the zeolite capped with hydrogen atoms (30).

The properties of supported metals can be tuned by adjusting the reactive atmosphere to regulate the fraction of the metal present as mononuclear complexes versus clusters. For example, the ratio of ethylene to $H_2$ in the gas environment regulated the ratio of mononuclear iridium complexes to $Ir_4$ clusters on dealuminated HY zeolite (32). The catalytic properties were changed by adjusting the relative amounts of the two forms of iridium, but in ethylene hydrogenation catalyzed by these species, the catalytic performance did not depend sensitively on the relative amounts of the complexes and clusters (33).

Markedly different results were observed when the metal was rhodium. For example, in the reactions of ethylene, the formation of clusters of only a few atoms of rhodium from the mononuclear species mentioned above caused the catalytic activity to increase 20-fold when the support was HY zeolite. The activity became so high that the hydrogenation swamped the dimerization, which was dominant when the rhodium was mononuclear. This is one of the few examples that clearly illustrate a tuning of the catalytic activity as the metal is switched between mononuclear complexes and clusters, but we anticipate that many others may exist, as discussed below.

Small, well-defined metal clusters on supports provide an opportunity for investigation of the nature of the metal–support interface. Vayssilov et al. (34) used DFT calculations to show that the metal atoms at the metal–support interface of zeolite-supported $Rh_6$ clusters are cationic, anchor the clusters to the support, and give the clusters a cationic character. That the metal atoms at the metal–support interface are cationic was suggested in 1991 on the basis of the metal–oxygen

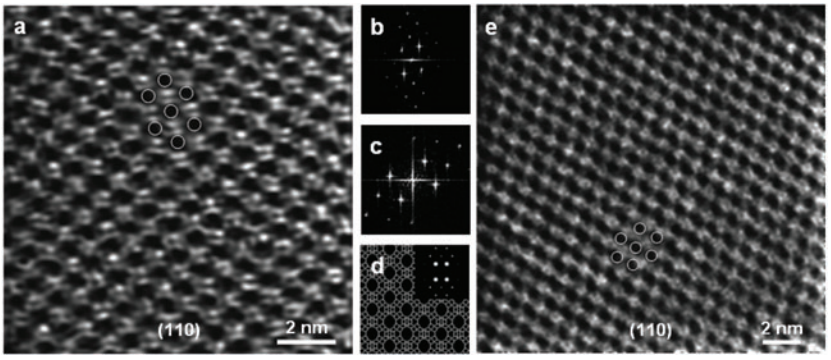


**Figure 5**

Images of atomically dispersed cationic gold in the supercages of zeolite NaY, a catalyst for CO oxidation at room temperature. Aberration-corrected high-angle annular dark field scanning transmission electron microscopy (ac-HAADF/STEM) images of a sample prepared by adsorption of $Au(CH_3)_2(acac)$ on the zeolite. (*a*) Initially prepared sample incorporating physisorbed gold complex. (*b*) Fast Fourier transform (FFT) of the experimental image shown in panel *a*. (*c*) FFT of the experimental image shown in panel *e*. (*d*) Simulated framework and theoretical diffraction pattern of zeolite Y in the [110] projection (*inset*). (*e*) Sample after treatment in flowing CO + $O_2$ (during CO oxidation catalysis) for 30 min, which led to a shifting in position of the Au atoms and a change in the gold ligation. Arrays of zeolite cavities with hexagonal arrangements are highlighted with white circles in panels *a* and *e*; these match precisely the simulated zeolite Y framework lattice in the [110] projection in panel *d*. For details and similar images, see Reference 38.

distances in oxide-supported metal cluster catalysts determined by EXAFS spectroscopy (35). The stabilization of metal clusters on supports by anchoring through metal ion–oxygen bonds may be general, and we address the point again below.

## Supported Gold Complexes

Gold that is highly dispersed on solid supports is an active catalyst for several reactions, including CO oxidation. The oxidation state of gold no doubt influences its catalytic activity, but because of the structural complexity of typical supported gold catalysts, the roles of zerovalent and ionic gold are not yet well resolved, as discussed below. Thus, samples were prepared to contain only cationic gold. $Au(CH_3)_2(acac)$ was adsorbed on zeolite NaY to give catalysts that were characterized by IR, EXAFS, and XANES spectra; the spectra showed that either $Au^{III}$ or $Au^{I}$ alone in the zeolite catalyzes CO oxidation (36, 37). Initially, $Au(CH_3)_2(acac)$ was physisorbed on the zeolite. When this sample was exposed to a mixture of CO + $O_2$ ($P_{CO} = P_{O2} = 11.7$ mbar) flowing at 298 K and 1 bar, catalytic oxidation to give $CO_2$ occurred. EXAFS spectra recorded during steady-state catalysis indicate the presence of mononuclear gold complexes. XANES and IR data indicate the presence of $Au^{III}$ and/or $Au^{I}$, and it was possible to tune the balance of $Au^{III}$ and $Au^{I}$ by controlling the ratio of CO to $O_2$ in the reactant stream—variation of the feed composition cycled the catalyst between forms. The cationic gold evidently constitutes well-defined catalytic sites; these have been imaged with STEM (38) (**Figure 5**).

# NOBLE METAL CATIONS AS ACTIVE CENTERS ON OXIDE SUPPORTS

In this section, we review recent literature pertinent to the identification of catalytically active sites comprising metal cations (M) stabilized on oxide supports; we represent such sites with

the shorthand M–$O_x$– and provide more evidence of the state of the metals below. Advances in the synthesis and characterization of catalyst surfaces with atomic-scale resolution and advanced computational methods have made the recent appreciation of this type of catalytic site possible.

In the late 1970s, Tauster et al. (39) coined the term strong-metal-support interaction to describe the apparent contribution of a (usually reducible) oxide support, such as $TiO_2$, to the catalytic site. It was later discovered that in some catalysts (e.g., $Pt/TiO_2$), the hydrogenation activity of platinum is decreased by a structural effect—a decoration or partial coverage of the active metal sites by reduced $TiO_x$ (40). The effect was evidently not primarily electronic.

However, the notion of strong metal-oxide–support interactions has resurfaced recently to explain how subnanometer clusters and even atoms or cations of a metal such as platinum survive often harsh reaction conditions and thermal treatments on some oxide supports. Exemplifying this point, Tanaka and coworkers (41, 42) have extolled the benefits of noble-metal-doped perovskites. These supports both stabilize the noble metal particles and maintain the metal in the oxidation states required to handle the competing demands of $NO_x$ reduction and oxidation of CO and hydrocarbons.

## Nanoscale Ceria as a Support of Platinum-Group Metal Cations

The introduction of ceria and in particular zirconia-doped ceria in the TWCs used in automobile exhaust converters was a tremendous success (43), as it provided catalysts with much better properties than the originally used $Pt/Al_2O_3$. The improvement was manifested especially after severe aging of the catalyst, which dramatically sinters the platinum particles and deactivates the catalyst. The strong interaction of platinum with ceria, exemplified by the enhanced reducibility of the surface oxygen of ceria upon metal addition, was recognized early as an indication of an electronic effect displayed by oxidized sites (Pt–$O_x$–Ce) (44), which were probably the active sites for the TWC redox chemistry. This effect was especially evident after catalyst aging, which in essence separated the metal into two parts—large platinum particles, which were inert in the reactions, and the nonmetallic part, which was presumably atomic or subnanometer oxidized $Pt_n$–O clusters strongly bound to the ceria surface. Clearly, ceria was more than a dispersant oxide support.

Raman spectra showed that rhodium, iridium, palladium, and platinum form surface-phase metal oxide (*M*–O) structures that interact strongly with the surface of $CeO_2$, whether the latter is in bulk form or present in microdomains within an alumina host structure (44, 45). Toyota researchers (46–49) showed that a reversible structural rearrangement of Pt–$O_x$–Ce species bound to ceria under cyclic redox conditions mimics the operation of a catalytic converter at approximately the stoichiometric air/fuel ratio. In essence, these researchers showed that the active Pt–$O_x$–Ce ensemble is under the influence of two push-pull forces: a reducing environment (rich condition) pulling and destabilizing the Pt–$O_x$ ensemble away from the cerium binding site and an oxidizing environment pushing the active Pt–$O_x$ ensemble back to the ceria. DFT calculations identified the stable configurations. Clearly, if one uses more platinum than this balance of forces dictates, under realistic conditions it will be lost (to sintering) as the new surface equilibrium is established—even if the platinum is initially present as well-dispersed nanoclusters. The amount of stable platinum under the high-temperature conditions characteristic of TWC operation is $\ll$1 wt% for aged ceria (47, 49) and is proportional to the number of surface oxygen defects of ceria that serve as anchoring sites, and the number of these sites depends on the $CeO_2$ crystal surface (50). The practical challenge becomes one of preparing nanoscale ceria with many surface oxygen defects, even after aging. The use of dopants such as zirconia, lanthana, and gadolinia in the ceria lattice achieves this goal (51).

The importance of the surface properties of ceria also is recognized for good design of catalysts employing dispersed platinum, palladium, gold, copper, nickel, and other metals for low-temperature applications. The reactions include oxidation of CO and of hydrocarbons (52, 53, 54, 55) as well as the water-gas shift (WGS) reaction (56, 57).

Gorte's group (58, 59) showed the difference between (low-activity) platinum, palladium, and rhodium supported on alumina or high-temperature-annealed ceria and (high-activity) platinum-group metals supported on low-temperature-annealed, high-surface-area ceria for both the CO oxidation and WGS reactions. A bifunctional catalyst site involves platinum that adsorbs CO, with ceria providing its labile oxygen in a Mars–van Krevelen–type mechanism; thus, a so-called redox mechanism for the WGS reaction was proposed. Although this mechanism does not specify the oxidation state of platinum or the reaction intermediates, it invokes a synergistic effect, whereby the properties of the ceria as a cocatalyst are as important as the metal catalyst.

Grabow et al. (60) reported a more detailed WGS mechanism for platinum, according to which $H_2O$ molecules first dissociate into OH and H species and then CO associates with the OH to form a fast-reacting carboxylate intermediate, which then releases the products $CO_2$ and $H_2$. Grabow et al. (60) and Meunier et al. (61) ruled out the alternative pathway involving a formate intermediate in the WGS reaction on platinum supported on ceria and on zirconia-doped ceria. Evidence linking the low-temperature WGS reaction on $Pt/CeO_2$ catalysts to a nonmetallic platinum species, $Pt–O_x–Ce$, was reported by Fu et al. (57), who showed that leaching of the platinum nanoparticles from the catalyst surface (e.g., by aqueous sodium cyanide solutions) and leaving only a fraction of the original platinum present on the ceria did not cause any drop in the WGS activity. X-ray photoelectron spectroscopy (XPS) was used to identify mainly $Pt^{II}$ and some $Pt^{IV}$, but no $Pt^0$ in the leached catalyst. A concerted mechanism for the WGS reaction was thus proposed that involves cationic platinum species in $Pt–O_x–Ce$ sites.

Similar findings were reported for $Au/CeO_2$ (57, 62) and $Cu/CeO_2$ (63, 64). The number of oxygen vacancy defects on the ceria surface was argued to be a crucial parameter determining the number of stabilized surface Pt cations. Pt cations adsorb CO less strongly than $Pt^0$ (65), and at near-ambient temperatures, they may be the only reaction-relevant sites for weak adsorption of CO.

Cationic palladium species represented as $Pd–O_x$ are associated with the active sites in supported palladium catalysts. $Pd/CeO_2$ catalysts show a temperature hysteresis associated with the decomposition of bulk PdO to give palladium metal at high temperatures and the reoxidation of palladium metal to $PdO_x$ at lower temperatures, as Farrauto et al. (66) first discussed in 1992. Similarly, Trovarelli's group (67) recently presented evidence suggesting the importance of an intermediate $PdO_x$ surface species. Unfortunately, this species, which initially was suggested in 1982 on the basis of TEM evidence of palladium particle sintering and redispersion (68), still has not been adequately characterized.

Observations made years ago established that rhodium undergoes a deleterious high-temperature interaction with alumina under oxidizing conditions (7, 69). Zirconia interacts weakly with rhodium, but ceria interacts strongly with it. Therefore, to preserve metallic rhodium in the automotive TWC, ceria-zirconia materials with high zirconia contents are used as the supports for rhodium. Rhodium is less noble than platinum or palladium in terms of its tendency to oxidize and react with supports. Ligthart et al. (70) demonstrated the strongly interactive nature of rhodium with ceria and its effect on CO oxidation. Although the supported rhodium species may not qualify as single-site catalysts, the occurrence of CO oxidation at least suggests that ceria and rhodium work in concert: the ceria evidently promotes the oxidation of small rhodium particles to stabilize $Rh–O_x$ as the active catalytic phase for CO oxidation, and this reaction is characterized by a TOF several orders of magnitude higher than that of (larger) metallic rhodium particles on ceria or

other supports. This result agrees with those of Somorjai and coworkers (71), who reported that the active phase in polymer-stabilized rhodium nanoparticles for CO oxidation is a thin surface oxide, the formation of which depends on the particle size. This is different from the bulk oxide, $Rh_2O_3$, which is inactive (72).

Synthesis techniques have been reported that aim at the preparation of embedded platinum, palladium, and other metals in ceria. Because of the partial solubility of precious metals in ceria, it is possible to prepare $Ce_{1-x}$–$Pt_x$–O and $Ce_{1-x}$–$Pd_x$–O solid solutions and to evaluate their activities and stabilities in various gas streams. For example, Hegde's group (73) used combustion of precursor salt solutions to prepare their catalysts. Depending on the gas composition and temperature, solid solution destabilization can take place, and platinum, palladium, and other metals can diffuse out of the bulk and form clusters of Pt–$O_x$, Pd–$O_x$, etc. bound on the ceria surface. Such a preparation may be a good way to create a larger number of active sites (M–$O_x$ linkages) on ceria. Similarly, diffusion of copper from the solid solution Cu–O–Ce reservoir takes place under reducing conditions to form surface clusters of Cu–$O_x$ on ceria, which are surmised to be the active sites for the low-temperature WGS reaction (64). To maximize the number of Pt–$O_x$–Ce linkages and suppress ceria nanoparticle sintering during calcination, coprecipitation accompanied by urea decomposition works well (74). Other synthesis methods such as strong electrostatic adsorption, which is suitable for monolayer metal deposition on supports, have the potential to stabilize Pt–$O_x$ and other M–$O_x$ sites on ceria and other supports (75). These methods should be examined and evaluated in detail.

## Pt–O and Pd–O on $FeO_x$ Surfaces

Similar to ceria, $Fe_2O_3$ can supply active surface oxygen to metals adsorbed on it. Liu et al. (76) reported that $FeO_x$ interacts strongly with platinum by modifying its electronic surface state. Addition of a monolayer of $Fe_2O_3$ (2%) to Pd/$CeO_2$ significantly enhanced the WGS reaction rate (77). It was proposed that oxygen from the iron oxide was transferred to the palladium, which lowered the barrier for oxygen transfer between $FeO_x$ and palladium and thereby enhanced the WGS reaction rate. The main requirement for this mechanism is that $Fe_2O_3$ be in close contact with palladium. This work did not examine the possibility that a layer of Pd–$O_x$ was stabilized on the $FeO_x$-modified $CeO_2$ surface.

Because Pt cations adsorb CO less strongly than $Pt^0$ (65), the low-temperature CO oxidation may be realized on surfaces containing atomic distributions of $Pt_n$–O species rather than metallic platinum nanoparticles. Thus, a flurry of recent research has characterized the system Pt–$FeO_x$ as a catalyst for CO oxidation and the preferential CO oxidation (PROX, which is selective CO oxidation in the presence of $H_2$) (78, 79).

Use of the $FeO_x$ support as a reservoir for oxygen to improve the activity of platinum for the PROX reaction under ambient conditions was demonstrated recently (78). The active site was surmised to be a highly reduced FeO layer on platinum; the reduced sites were replenished by the excess hydrogen present in the PROX reaction. The possibility of a contribution of subsurface iron, proposed in earlier work by the same group, still holds (79), however.

Li et al. (80) reported that Pt/$Fe_2O_3$ prepared by a colloid-deposition method under wet conditions is active for CO oxidation. Liu et al. (81) recently used ferric hydroxide as a support; a combination of platinum and palladium on $Fe(OH)_x$ facilitates $Fe^{3+}$ reduction and hydroxyl loss at relatively low temperatures, which leads to the production of many oxygen vacancies. Significant activity at room temperature was demonstrated for the Pt/$FeO_x$ catalyst, but platinum was present in a variety of species on the surface, which hindered the identification of the active species.

To elucidate the nature of the catalytic sites, Qiao et al. (82) used very low loadings of platinum with a high-surface-area $FeO_x$ support to show that it is possible to maintain the platinum as well-separated cations on the oxide surface and that these do not change with time-on-stream in the catalytic CO oxidation reaction. Using STEM and XANES spectroscopy, the authors clearly observed Pt cations substituted into the $FeO_x$ lattice and occupying exactly the positions of the Fe atoms. At higher platinum loadings, mixtures of single Pt atoms, 2D platinum rafts consisting of fewer than 10 Pt atoms, and 3D platinum clusters approximately 1 nm or less in diameter were observed by STEM. The ambient-temperature CO oxidation activity of the individual Pt cations stabilized on the $FeO_x$ was established in this work. Even the used catalyst contained cationic platinum; no Pt–Pt coordination was found by EXAFS spectroscopy. This work constitutes a description of one of the best-defined atomically dispersed noble metal catalysts on an oxide. In contrast to the zeolite-supported metal complexes described above (e.g., the rhodium dicarbonyl shown in **Figure 1**), the platinum is evidently in the support rather than on it, and in contrast to samples such as that represented in **Figure 1**, the ligand environment of the metal is not defined.

The conclusion from the above work—that atomically dispersed Pt–O species serve as single-site surface catalytic centers—is opposite to the conclusion in another 2011 report ruling out cationic platinum in Pt–O sites on $FeO_x$ as the active centers for CO oxidation (83). An issue with this report, however, is the lack of detailed spectroscopic analysis of what comprises the interface between the colloidal platinum particles and the $FeO_x$ phase. Reconciliation of the two reports might be expected upon clarification of this point.

## Platinum Cations on Alumina and Silica: What Keeps Them Bound?

Murrell et al. (45) proposed that a layer of Pt–O– formed and stabilized very close to the ceria surface (within 1 nm) can explain the activity of Pt–O– species on other supports as well. This structure can operate by a Mars–van Krevelen mechanism involving the terminal O on the Pt cations. In the process, platinum switches rapidly from $Pt^{II}$ to $Pt^0$ and back. Whereas ceria can stabilize many such structures, other oxide surfaces are more or less able to do the same. This alternative has not yet been considered in the literature, although recent findings about the structure of a Pt–O layer on $FeO_x$ (78), discussed above, may soon change the situation. Significantly, a Pt–O–Pt–O– layer held very close to the surface has been reported for $\gamma$-$Al_2O_3$ enriched with 5-coordinated $Al^{3+}$, the latter identified by NMR spectroscopy (84). Thus, a common Pt–O– species bound to (as yet undefined) minority sites on oxide surfaces is emerging, aided tremendously by atomic-resolution STEM imaging.

Addition of alkali oxides to Pt/$\gamma$-$Al_2O_3$ and even to Pt/$SiO_2$ surfaces is effective in creating active WGS reaction sites comprising Pt–O and neighboring –OH groups that could activate CO at temperatures as low as 100°C, similar to the Pt–O– sites on ceria (85). The active site stabilizes platinum as well as the alkali metal ions that are bound to Pt–O. Repeated washings of the catalyst with deionized water at ambient temperature or 70°C do not remove these alkali ions. **Figure 6** shows the activity of sodium-promoted atomically dispersed platinum on a $SiO_2$ surface. The catalytic site was stable in realistic WGS gas streams, and platinum retained its oxidized state, as shown by XANES of the catalyst operating at 275°C. On the basis of ab initio molecular dynamics calculations (85), a few plausible structures of the active site were proposed for the potassium-promoted platinum. The cluster $PtK_6O_4(OH)_2$ retains platinum in an oxidized state with a K:O ratio of 1:1; it binds CO weakly, and it adsorbs/dissociates $H_2O$ almost without any energy demand—similar to Cu(111), arguably the best WGS catalyst (86).

Whether alkali-promoted or not, and irrespective of the choice of support, all platinum catalysts that are active for the low-temperature WGS reaction are characterized by similar apparent

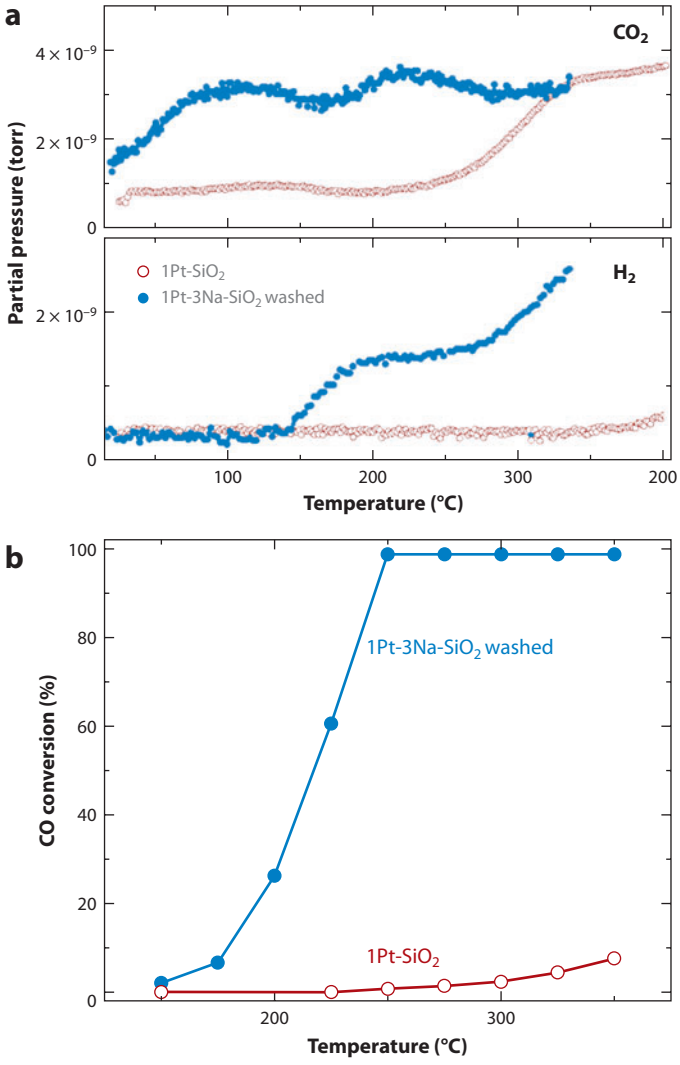


**Figure 6**

Sodium promotion of $Pt/SiO_2$ for the low-temperature water-gas shift (WGS) reaction. The promoted Pt-O-$Na(OH)_x$ sample includes nonwashable sodium. (*a*) Temperature-programmed reduction with CO shows the onset of OH activation by CO at ~100°C, accompanied by the production of $H_2$ and $CO_2$. The first $CO_2$ peak is from adsorbed oxygen species; it is not relevant to the WGS reaction (85). (*b*) Steady-state conversion of CO measured in 2%CO-10%$H_2O$-He gas mixture; contact time: 0.09 g s $cm^{-3}$ (85).

activation energies, 70 ± 5 kJ $mol^{-1}$ (57, 60, 74, 85). Therefore, the key steps of the WGS reaction (CO adsorption and $H_2O$ activation) were proposed to occur on Pt–$O_x$–$(OH)_y$ sites, irrespective of the type of support and the additive (85). When Pt–O– species are present on inert supports such as silica or alumina, the alkali metal addition provides the stabilization and brings OH groups to the site, as on ceria surfaces.

Yoshida et al. (87), by using in situ XANES and temperature-programmed desorption of oxygen under the influence of heating under oxidizing conditions, found that basic oxide supports stabilize platinum in high oxidation states. The platinum particles on MgO were redispersed and stabilized

through the formation of atomically dispersed platinate anions comprising tetravalent Pt cations coordinated by oxygen anions.

In summary, mononuclear ensembles consisting of cationic rhodium, palladium, platinum, and other metals anchored to supports through M–O linkages can be formed and stabilized on supports in configurations that are stable and active for several reactions, notably including the redox reactions described here. Much remains to be learned about the structures of these surface species.

## GOLD CATIONS AS CATALYTIC CENTERS ON OXIDE SUPPORTS

Research on the automotive TWC and its continual improvements has contributed significantly to our understanding of the interactions of platinum-group metals with oxide supports. Our understanding of catalysts containing presumably analogous Au–O structures is still emerging. Historically, gold was realized to be an active catalyst much later than platinum; the first reports by Galvagno & Parravano (88) and Bond & Sermon (89) date back only a few decades. As Haruta et al. (90) first pointed out in 1987, only when gold is present in nanoscale structures is it an active catalyst. It can then be an extremely active CO oxidation catalyst, capable of converting CO to $CO_2$ at −70°C (91), depending on the support, the gold dispersion, and the reaction environment. Although the stability of gold supported on various oxides is generally inferior to that of platinum and the two metals have totally different electronic properties, it is fundamentally interesting to examine whether the two share any common properties and structures in their atomic-scale interactions with oxide surfaces.

### Au–$O_x$ Catalytic Species in the CO Oxidation Reaction

Following Haruta et al.'s (91, 92) discovery of the extremely high CO oxidation activity of nanoscale gold on $TiO_2$, $\alpha$-$Fe_2O_3$, $Co_3O_4$, and other reducible metal oxides, numerous researchers joined this field of research, leading to reports of other reactions catalyzed by nanoscale gold. One of them, the hydrochlorination of acetylene on gold, was reported by Hutchings and colleagues (93) simultaneously with Haruta's first report of CO oxidation on nanogold. By 1997, Haruta and colleagues (94) had compiled a substantial list of reactions for which gold showed activity, and numerous researchers have added to the list, notably including Corma and colleagues (95, 96). Several comprehensive reviews (97–99) summarize the literature up to 2006.

Here, we review recent reports in which atomically dispersed gold appears to be part of the catalytic site. The following section links with the Supported Gold Complexes section concerned with zeolite-supported mononuclear cationic gold catalysts for CO oxidation.

The fascination with the seemingly simple CO oxidation reaction catalyzed by highly dispersed gold has continued unabated for 20 years. What is the active state of gold? Better stated: what are the active states of gold? How small should gold clusters be to be most active? Are gold clusters active alone?

$Au(CH_3)_2(acac)$ was used to prepare gold catalysts supported on high-area nanostructured lanthana (100). This catalyst was used for CO oxidation at 298 K and 1 bar, with an unusually high (5:1) stoichiometric excess of $O_2$ fed with CO to a flow reactor. The catalyst had an activity comparable with that of the most active supported gold catalysts under those conditions. XANES of the working catalyst demonstrated that the gold was present as $Au^{III}$; EXAFS spectra were consistent with the presence of mononuclear gold complexes. Presumably, the isolated gold cations were engaged in the catalysis, but details of the role of the support are lacking. The excess of $O_2$ likely stabilized the $Au^{III}$. This catalyst is evidently related to the zeolite-supported catalyst mentioned

in the Supported Gold Complexes section but substantially different from those incorporating gold clusters, as described below.

A breakthrough in the 1990s was the realization that 3D and 2D gold clusters on $TiO_2$ have different activities (101). STEM images were used to infer that ~0.5-nm-diameter bilayers of 10-atom gold clusters are more active for CO oxidation on $FeO_x$ than single atoms or larger clusters (102). However, according to Bond & Thompson (98), the chemical glue that keeps the gold bound to the support and the possible importance of the peripheral gold sites and cationic gold sites for the CO oxidation activity have been much harder to delineate.

Liu et al. (52, 53) reported that $Au/CeO_2$ prepared by coprecipitation with the citrate complexation method was the most active CO oxidation metal on ceria. Several years later, Corma's group (103) found that gold deposited on ceria nanoparticles was two orders of magnitude more active than the same amount of gold on microcrystalline ceria. The activity derived from $Au–O_x–$ species at the interface with ceria was hard to evaluate in this system because of the large amount of gold present as nanoparticles. However, cationic gold, identified by XANES spectra, was inferred to have been present at the gold cluster–support interface and was implicated in the catalysis, which also benefited from the surface chemistry of the nanostructured ceria stabilizing superoxide adspecies (104).

Similarly, ceria-supported gold catalysts were prepared from $Au(CH_3)_2(acac)$ and used for CO oxidation in flow reactors with a $CO:O_2$ molar ratio of 0.5. The catalyst was found by EXAFS spectroscopy initially to incorporate mononuclear gold complexes. As it functioned in the flow reactors serving as spectroscopic cells, the gold underwent reduction (as shown by XANES spectra of the working catalyst) and aggregation to give clusters that grew in nuclearity to approximately 30 atoms each, on average (as shown by EXAFS spectra). Simultaneously, the catalytic activity under stoichiometric reaction conditions increased dramatically (105). The data show that the gold clusters or gold at the cluster–support interface give catalysts that are much more active than mononuclear gold complexes on high–surface area ceria.

Some researchers earlier used theory to infer that CO oxidation on gold nanoparticles is independent of support effects (106) and that low-coordination atoms on the nanoparticles are the active sites. We consider these results to be insufficient to account for the complexity of catalysis by supported gold. The conclusion does not account for the observations of catalysis by mononuclear gold complexes and the roles played by supports, such as ceria, that stabilize reaction intermediates such as superoxides or peroxides.

We might at least begin to reconcile these observations with the hypothesis (107) that multiple energetically favorable reaction channels exist for CO oxidation involving gold. Notwithstanding the stoichiometric simplicity of the reaction, the occurrence of catalysis at low temperatures, and the value of the reactant CO as a probe of catalyst structure in experiments such as IR spectroscopy, this test reaction is evidently not as valuable in providing insights into the catalytic action of gold as many hoped it might be.

Consistent with the inference of multiple reaction channels for gold-catalyzed CO oxidation, the Flytzani-Stephanopoulos group (108) recently showed that unsupported gold clusters in solution can catalyze this reaction under ambient conditions. Gold clusters and nanoparticles with average diameters <2.5 nm were stabilized in solution by various poly(amidoamine) dendrimers. The activity of the freshly prepared dendrimer-encapsulated gold nanoparticles was low, but it increased drastically with storage time. The gold particle size distribution did not change with aging; rather, activation of the catalyst took place via partial hydrolysis of gold, as shown by UV-VIS spectroscopy. Thus, oxidized gold species and in particular $Au(OH)_x$ species were indispensible to activate the CO oxidation reaction in solution. The reported activity was of the same order of magnitude as that of a highly active $Au/TiO_2$ catalyst (109).

In the case of oxide-supported gold, the interfacial (basal) atoms can be oxidized, and the support oxygen defects may then be crucial to nucleate and stabilize the active gold phase. Recent research has provided additional evidence of the role of the gold–ceria interface for the CO oxidation reaction; data were obtained with a catalyst constructed layer by layer, $CeO_2$/Au/$CeO_2$/Au/. . ., on silicon wafers in an electron-beam apparatus (110). When $CeO_2$ and gold nanolayers were separated by $SiO_2$ interlayers, the nanotowers were totally inactive, but in the absence of these interlayers, the catalyst was active. Activity was similar for different gold layer thicknesses. Thus, the active sites reside at the interfaces of gold and ceria (110). Using model catalysts prepared as inverse structures [i.e., $CeO_2$ islands vapor deposited on Au(111) surfaces and imaged by scanning tunneling microscopy (STM)], Rodriguez et al. (111) also showed the importance of the gold–ceria interface for the WGS reaction. In both approaches, what exactly comprises this active interface could not be determined with the characterization techniques applied.

Recently, on the basis of STM and XPS data characterizing $CeO_2$(111), Baron et al. (112) argued that the $Ce^{4+}$ concentration in nanostructured ceria thin films decreased after deposition of gold, and they observed simultaneously a significant concentration of oxidized gold species. These observations agree with the results of Zhou et al. (113), who used XPS to characterize the inverse structure of electron-beam deposited $CeO_2$ islands on polycrystalline gold films and reported a high $Ce^{3+}$ content (∼35%) in these materials.

By applying in situ Raman spectroscopy, Herman's group (114) monitored the oxygen vacancy concentrations on ceria during the oxidation of CO on $CeO_{2-\delta}$ nanorods and Au-$CeO_{2-\delta}$ nanorods, nanocubes, and nanopolyhedra. The first-order $CeO_2$ $F_{2g}$ peak near 460 $cm^{-1}$ decreased in intensity when the CO reaction was fast (fast reduction and relatively slow reoxidation of the surface) because of the lattice expansion that occurs when $Ce^{3+}$ replaces $Ce^{4+}$ during the creation of oxygen vacancies. The nonstoichiometry increased for the most active catalyst, Au-$CeO_{2-\delta}$ nanorods, for which $\delta \sim 0.04$ was measured.

On the basis of our earlier discussion about the importance of a Pt–O structure bound to supports, we now pose the same question about gold: do Au–$O_x$ phases exist that are similar to the Pt–$O_x$ phases that are part of the active sites for CO oxidation, the WGS reaction, and other low-temperature oxidation reactions? Recent evidence raises some key questions: Corma's group (103) inferred that, in CO oxidation catalyzed by gold supported on nanostructured $CeO_2$, the support provides reactive oxygen to the active gold species at the gold–support interface. Yates and coworkers (115) reported a different route for the reaction on $TiO_2$-supported gold. These authors also inferred a dual catalytic site, Au–Ti, at the perimeter of 3-nm-diameter gold particles, using IR spectra and DFT calculations to conclude that diffusion on the $TiO_2$ surface initially delivers CO molecules on $TiO_2$ sites to the active perimeter sites, where they assist O–O bond dissociation and react with oxygen. Thus, CO is postulated to attack an Au–OO–Ti species at the interface to form $CO_2$, and gaseous $O_2$ regenerates the Ti–OO species. This pathway involves the $TiO_2$ and the Au–O species at the interface; it does not involve CO adsorbed on gold nanoparticles. The oxidation state of gold at the interface was not specified in this work (and in Corma and coworkers' work cationic gold was postulated).

Fugitani & Nakamura (116) arrived at conclusions similar to those of Yates et al., namely, there is a low-temperature (<∼50°C) reaction pathway for CO oxidation that involves only the Au atoms located at the periphery of the gold particles attached to $TiO_2$, and the catalytic activity for CO oxidation correlates neither with a change in the fraction of edge or corner sites nor with a change in the electronic structure of the gold particles induced by quantum size effects. At temperatures greater than ∼50°C, the mechanism switches to one involving CO adsorption sites on the gold nanoparticles. But, in contrast to Green et al. (115), these researchers found that $H_2O$ plays an essential role in promoting the oxidation of CO at temperatures less than ∼50°C.

CO is oxidized to $CO_2$ by a hydroperoxide species that the reaction of $O_2$ with $H_2O$ can produce directly (117, 118). The O–O bond in the hydroperoxide species is activated, and consequently the reaction with CO to form $CO_2$ occurs with a low activation barrier.

Earlier reports by Haruta's group (119) and others (120, 121) had invoked OH as a necessary part of the CO oxidation reaction mechanism. Similar hypotheses were offered when the supported gold was used in aqueous solutions for CO oxidation (122) and for selective oxidation reactions (123).

Although OH may or may not participate in the CO oxidation reaction pathway, a hydroxylated support is desirable to stabilize gold clusters, primarily for the dry CO oxidation reaction, whereby gold destabilization (e.g., on $TiO_2$) takes place even during storage (124). Veith et al. (124, 125) found that surface hydroxyl groups were essential for stabilizing gold clusters on $TiO_2$ against coarsening under ambient conditions. Haruta's group reported that a hydroxide, $AuLa_2(OH)_9$, which was prepared by coprecipitation, showed markedly high catalytic activity for CO oxidation at a temperature as low as −80°C after reduction at 100°C (126). The catalyst mainly consisted of $Au^0$ clusters smaller than 1.5 nm in diameter, which were well mixed with $La(OH)_3$ containing isolated $Au(OH)_3$ species. Haruta and colleagues proposed that the size requirement of the gold species is strict and that the cluster diameter should be far less than 2 nm for CO oxidation activity to be realized.

In other work, Gluhoi & Nieuwenhuys (127) used alkali/alkaline earth metals as structural promoters to stabilize gold clusters in the PROX reaction. However, not everyone agrees on the role of hydroxyl groups or alkali and alkaline earth metals in dispersing gold species on oxide supports. For example, Hutchings and coworkers (102) reported that surface hydroxyl groups on FeOOH enhanced the coarsening of the gold particles.

Several questions remain open about the interplay between gold clusters, isolated cationic gold complexes, and gold (that may be cationic) at the gold cluster–support interface. To some degree at least, the isolated gold complexes and gold clusters on supports can be reversibly converted to each other, as shown by the results of IR and X-ray absorption spectroscopies (128). Intriguingly, $CO_2$ oxidized gold clusters on lanthana more readily than $O_2$, possibly by dissociating on the gold to give CO and reactive O species on the surface that do not form $O_2$. These observations suggest that CO oxidation catalyzed by $O_2$ may be autocatalytic under some conditions. NO is an even more efficient oxidant of gold clusters than $CO_2$. These results suggest opportunities for using $CO_2$ and NO as coreactants in various gold-catalyzed reactions.

In summary, the literature regarding CO oxidation catalyzed by gold is complex and unresolved. In answer to the question about the identities of the active states of gold, we hypothesize that multiple such states exist including interfacial gold and cationic gold. Regarding the question about how small gold clusters should be for maximum activity, we suggest that, at least in some cases, the size may be that which gives the maximum number of peripheral Au atoms. And in response to the question of whether gold clusters alone are active, we do not rule out the possibility but suggest with some generality that there is more to an active gold catalyst for CO oxidation than gold clusters. Extensive evidence exists for the role of cationic gold, for the participation of gold at the interface between gold clusters and supports, for the role of supports in addition to those affecting the gold–support interface, and for the role of support groups such as OH groups and sites where other reactive intermediates can form.

## Gold Cations in the Water-Gas Shift Reaction

The Andreeva group in 1996 (129) and the Flytzani-Stephanopoulos group in 2001 (130) first reported the low-temperature WGS activity of supported nanostructured gold for $Au/Fe_2O_3$

and $Au/CeO_2$, respectively. Both groups identified an important role of the support. Over the following decade, the same groups and others have pointed out the importance of specific oxygen sites of the support oxide surface that are needed to anchor and stabilize the active gold sites. For example, $FeO(OH)_x$ surfaces are necessary for the preparation of active $Au/FeO_x$ catalysts (131); in contrast, the surface oxygen vacancies of ceria were proposed as the loci for anchoring $Au_n$–O species (57, 62, 132, 133).

In a 2003 paper, Fu et al. (57) used a NaCN leaching solution to remove metallic gold nanoparticles and other weakly bound gold species from ceria. Heat treatment in air was then used to remove any cyanide species from the surface. The residual gold species (~10% of the original amount) on the surface were oxidized, as shown by XPS, and single-site gold cations were later found by XANES/EXAFS spectroscopy on these materials (134). The leached and parent materials exhibited identical WGS activity, which implies that only the residual cationic gold species associated with ceria, as $Au–O_x–Ce$, were active for the WGS reaction. On the basis of DFT calculations, King's group (133) later modeled this site as a small positively charged cluster of four Au atoms surrounded by six oxygen atoms over an oxygen vacancy of $CeO_2(111)$. This multinuclear Au–O site had high activity for the WGS reaction. In their DFT calculations characterizing $CeO_2(111)$ slab models, Castellani et al. (135) favored deposition of gold on oxygen atoms on various facets of ceria, which resulted in either neutral or oxidized gold species.

Conflicting assignments of the charge of gold clusters on ceria have appeared. The suggestions have ranged from negative to positive and even neutral species (62, 133, 136–138). Some of the reported assignments are ambiguous, however, because of the presence of all types of gold structures (atoms, clusters, and nanoparticles) in most of the examined catalysts.

To clarify the roles of various gold species, Deng et al. (134) examined a leached $Au/CeO_x$ catalyst for the WGS reaction using in situ XANES/EXAFS spectroscopy. Starting from a fully dispersed gold state, for which no Au–Au contributions were evident and only an Au–O coordination was observed by EXAFS spectroscopy, they followed the evolution of the gold structure under reaction conditions. The oxidation state of gold depended on the reaction gas composition and the temperature. The higher the temperature or the more reducing the reaction gas mixture, the less oxidized were the gold species. As the number of oxidized gold species dropped and gold aggregation took place, a loss of catalytic activity occurred. Hence, gold destabilization away from the $Au–O_x–Ce$ active site caused the deactivation (134), in contrast to the results mentioned above for ceria-supported gold catalysts for CO oxidation under stoichiometric conditions (105). The gold destabilization was reversible (i.e., redispersion of gold onto the ceria surface was possible through oxidation at 400°C by gaseous $O_2$, accompanied by an increase in surface oxygen and recovery of catalytic activity). These findings establish the $Au–O_x–Ce$ species as the active site for the low-temperature WGS reaction, and they can guide the design of gold/ceria catalysts and the choice of processing conditions [e.g., addition of small amounts of $O_2$ to the reformate gas can suppress the destabilization/reduction of Au–O species and prolong the gold catalyst lifetime (139)].

Deng et al. (140) further compared the WGS reaction kinetics in the reaction catalyzed by $Au/CeO_2$ and that by $Au/FeO_x$, the latter with a commercial 2.2 at% $Au/Fe_2O_3$ catalyst and its CN-leached derivative, which contained only 0.7 at% $Au/Fe_2O_3$ and comprised only isolated subsurface gold cations after leaching and air calcination at 400°C. The reaction rates normalized to the specific catalyst surface area were similar for the $CeO_2$- and $FeO_x$-supported gold catalysts. They were also the same for the parent and leached catalysts, and the apparent activation energy of the reaction was the same for each catalyst; all this evidence provides strong support for the inference that the active sites are the atomically dispersed $Au–O_x–Ce$ and $Au–O_x–Fe$ surface species.

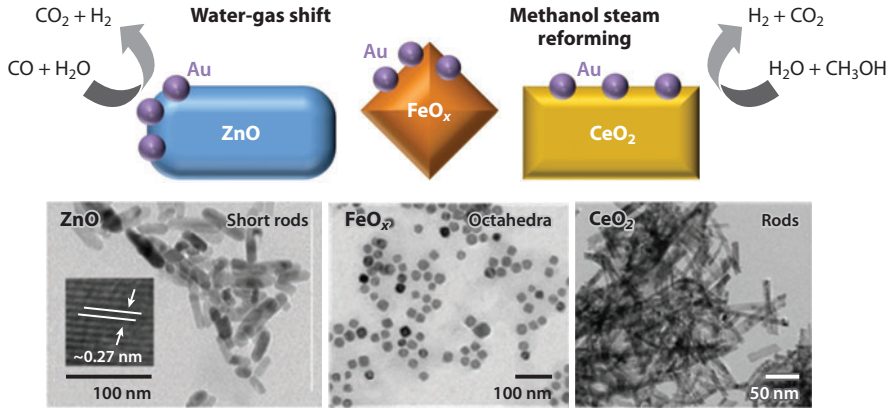


**Figure 7**

Shape effect of nanocrystals of $CeO_2$, $Fe_3O_4$, and ZnO on the binding of active Au–O species for the water-gas shift and methanol steam reforming reactions (142). Reproduced by permission of the PCCP Owner Societies.

The evolution of the gold structures active for the WGS reaction in leached Au–$Fe_2O_3$ samples was examined by in situ XANES and EXAFS spectroscopy. Findings were similar to those reported for the Au–$CeO_2$ catalyst; namely, conversion of Au–O species to gold clusters with time-on-stream took place with concomitant catalyst deactivation (Y. Zhai, Y. Wang, B. Zugic, and M. Flytzani-Stephanopoulos, unpublished observations). Redispersion of gold by treatment in $O_2$ at 400°C led to recovery of the activity. Therefore, a common active site seems to have been present on both types of supports involving an ensemble of Au–O– species.

The potential shape effects of ceria were investigated by depositing 1% gold on ceria nanostructures with various shapes (rods, cubes, and polyhedra) prepared as single crystals by hydrothermal methods (141). Whereas gold on the ceria nanocubes {100} was poorly dispersed and formed nanoparticles (average 3 nm in diameter), most of the gold on the {110} facets of the ceria nanorods was atomically dispersed. The former was inactive, whereas the latter was highly active for the low-temperature WGS reaction. After leaching, 0.03% and 0.6% gold remained on the catalysts, respectively. The TOF (based on the residual gold) was the same for the two catalysts. Hence, the ceria shape effect is evidently indirect—it manifests itself only as a collection of binding sites for gold, many for the {110} but few for the {100} polar surfaces of ceria (141). To maximize the number of atomically dispersed active gold sites, various single crystals of the support oxide were prepared at the nanoscale, as shown schematically in **Figure 7** for ceria and for nano-$Fe_3O_4$ and nano-ZnO single crystals (142).

Significantly, a similar indirect effect of ceria shapes on Au–O was found when this type of catalyst was used for methanol decomposition and methanol steam reforming reactions (143, 144). For methanol reactions on gold, all the available evidence points again to Au–O species as the active sites; hence, the $CeO_2$ {110} surfaces that can disperse gold atomically are superior to ceria nanocubes presenting {100} surfaces (143, 144). Working with Au/nano-ZnO shapes, Boucher et al. (142, 145) found the polar surfaces of ZnO {0001} to be the best supports for the active gold sites. In addition, the WGS reaction on Au/$FeO_x$ catalysts depended on the iron oxide shape in experiments with gold deposited on single crystals of nano-$Fe_3O_4$, (i.e., octahedra {111} and cubes {100}) (142).

On the basis of the above discussion, we infer that atomic distributions of gold on oxides are important for the WGS reaction, and it should be possible to detect them by various advanced

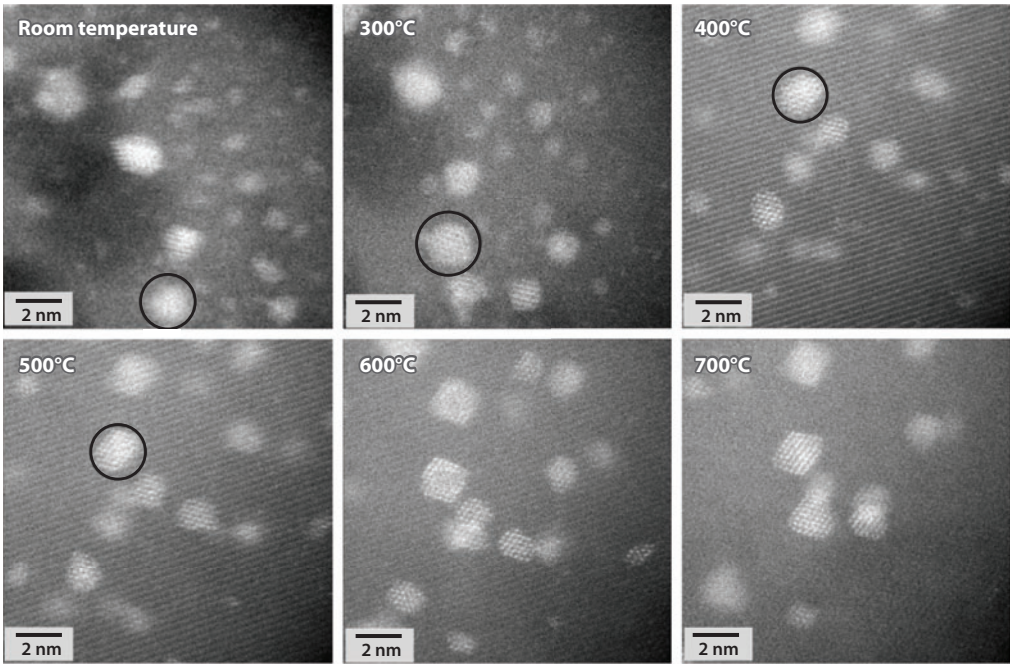


**Figure 8**

Aberration-corrected high-angle annular dark field scanning transmission electron microscopy (ac-HAADF/STEM) images of used 0.7 at% Au/$FeO_x$ (NaCN-leached, 400°C-air calcined sample from parent World Gold Council-2.2 at% Au/$Fe_2O_3$). The sample was annealed sequentially to increasingly higher temperatures in the microscope (146).

techniques. Thus, using atomic-resolution electron microscopy, Allard et al. (146) examined NaCN-leached Au–$Fe_2O_3$ materials and found them to contain a preponderance of gold cations. These gold cations were present not only in the fresh, leached sample after air calcination at 400°C but also in the sample used for the WGS reaction at temperatures up to 350°C and even in a sample treated in $H_2$ at 400°C. The latter also incorporated several subnanometer and nanometer-sized gold clusters. Allard et al. (146, 147) showed that the Au–$FeO_x$ interaction is quite strong. In a series of in situ heating tests in the microscope at temperatures up to 700°C, gold sintering did not begin at temperatures less than 500°C, and even at 700°C, the gold clusters were less than 2 nm in diameter (**Figure 8**).

To elucidate the nature of the interaction of atomically dispersed gold with a support surface, model catalysts can be investigated in a controlled, ultrahigh vacuum environment. Thus, Rim et al. (148) prepared a submonolayer of Au adatoms on an Fe-terminated $Fe_3O_4$ (111) single-crystal surface to investigate the site-specific adsorption of Au adatoms using STM and scanning tunneling spectroscopy. Au adatoms preferentially bound on the uncapped oxygen atoms were positively charged and were the exclusive sites for CO adsorption at 260 K (**Figure 9**). In more recent work (K.T. Rim, J.M. Raitano, S.W. Chan, M. Flytzani-Stephanopoulos, and G.W. Flynn, unpublished observations), the same group investigated the adsorption of water molecules on $Fe_3O_4$ (111) and found that –OH adsorbs preferentially on the terminal Fe atoms surrounding the uncapped oxygen. Pending experimental evidence, we speculate that an ensemble of Au–$O_x(OH)_y$–Fe contains the active sites for the WGS reaction on Au/$FeO_x$ surfaces.

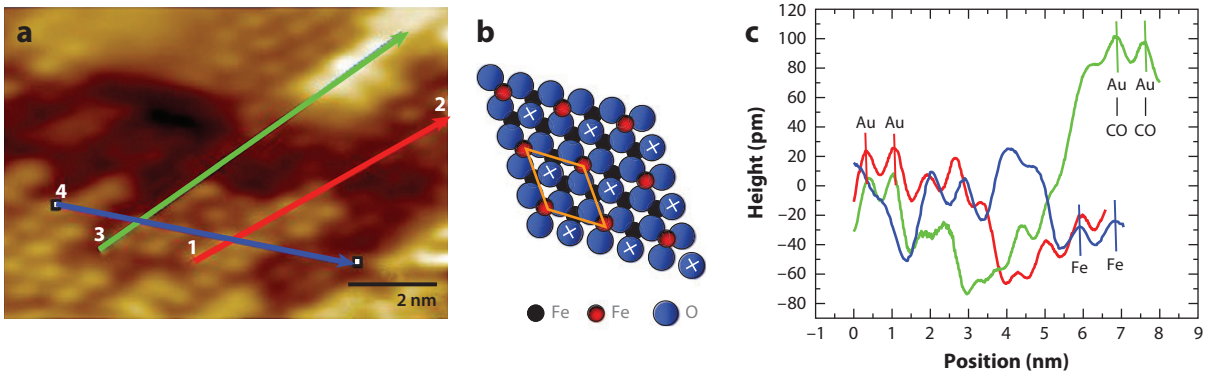


**Figure 9**

(*a*) Scanning tunneling microscopy (STM) and spectroscopy (STS) of CO adsorbed on Au adatoms on an Fe-terminated $Fe_3O_4$ (111) single crystal at 260 K. (*b*) A model of the a Fe-terminated $Fe_3O_4$ (111) single crystal; X indicates an uncapped oxygen atom. (*c*) Vertically bound CO on the Au adatoms and not on the Fe atoms is shown by STS. Color traces correspond to line scans in panel *a*. Height difference between Au-Au adatoms and surface Fe-Fe atoms is 0.4–0.8 Å (*blue* and *red* line scans in panel *a*). The height difference between Au adatoms and CO is 0.6–0.8 Å, corresponding to the brightest feature in the green line scan in panel *a* (148).



Ribeiro's group (149) recently used a physical model of gold nanoparticles present as cubo-octahedra on $TiO_2$ to obtain results leading to the claim that corner atoms with fewer than seven neighboring Au atoms are the dominant active sites for the low-temperature WGS reaction. The number of corner sites does not vary as particle diameter increases to more than 1 nm, which leads to the surprising result that the rate per gold cluster is independent of size. However, subnanometer clusters were not evaluated in that work, and different fits of the rate with the gold particle size could be used—that is, a size-independent rate for diameters exceeding ~2 nm could be inferred. Leaching of the gold should be used to check whether, as in the case of $Au/CeO_2$ and $Au/FeO_x$, the atomic Au–O species (basal or peripheral atoms) are the active WGS sites on $TiO_2$ as well. Hence, the proposed activity–Au particle size correlation does not constitute an irrefutable demonstration of the reaction-relevant gold species.

## Gold Cations in Ethylene Hydrogenation

Atomically dispersed gold on open oxide supports can be prepared by methods other than the two-step method (with leaching as the second step as discussed in the previous section). Prominent among them is the vapor-phase deposition or adsorption from the liquid phase of organometallic precursors, such as the $Au(CH_3)_2(acac)$ used by Guzman & Gates (150, 151), notably on MgO. The synthesis is similar to that described above for precursors such as $Ir(C_2H_4)_2(acac)$ and zeolite supports. We mention briefly here the use of this approach to investigate ethylene hydrogenation catalyzed by supported gold, as the results tie to those presented above for zeolite-supported catalysts.

A family of MgO-supported samples was prepared, and the activity for ethylene hydrogenation was determined as a function of the Au–Au coordination number determined by EXAFS spectroscopy (150). The catalyst had maximum activity at the onset of the reaction, when only gold cations were present on the MgO surface. The isolated cations were imaged with STEM (152). In situ EXAFS spectroscopy showed that as gold clusters formed during the reaction, the activity decreased; gold clusters were inferred to be inactive.

## CONCLUDING REMARKS

A consensus regarding the mechanism of CO oxidation and the WGS reaction on single-site multinuclear ensembles of gold or platinum on open supports has not been reached, but one seems under slow construction. Remarkably, the much-investigated CO oxidation reaction is the most challenging mechanistically, whereas for the WGS reaction, the preponderance of evidence points to the cationic Pt–O– and Au–O– species as the active sites. Other reactions may be similarly examined. A change in mind frame is needed to accept that for some reactions, atomically dispersed M–O species are the active sites or at least are involved in the active sites, and that this is true not only for reactions on well-defined samples, as illustrated by zeolite-supported catalysts (which seems to be rather well accepted), but even for reactions on open supports.

At this time, a few good, reproducible preparation methods are clearly needed to prepare exclusively atomic dispersions of gold, platinum, or other noble metals on supports other than zeolites as well as to stabilize them with well-defined anchoring ligands such as –O or –OH. Promoter ions, such as alkali and alkaline earth metal ions, may be used to stabilize the noble metal sites. To maximize the catalytic reaction rate, the number of active, atomically dispersed metal sites will have to be maximized. As shown in the Gold Cations in the Water-Gas Shift Reaction section, this goal can be met on specific single crystals of the support oxide that can be prepared at the nanoscale by hydrothermal and other synthesis methods. Similar suggestions can be made for other metal cations. Materials related to the zeolite-supported samples mentioned above might provide analogs for catalyst preparation on open supports. Characterization of such well-defined structures (without reliance on the average structural data that are often the best available for structurally complex catalysts) is expected to facilitate incisive understanding of working catalysts in the absence of interference from structures that do not play a catalytic role, which often include metal clusters and nanoparticles.



## DISCLOSURE STATEMENT

The authors are not aware of any affiliations, memberships, funding, or financial holdings that might be perceived as affecting the objectivity of this review.

## ACKNOWLEDGMENTS

The coauthors acknowledge the U.S. Department of Energy, Office of Science, Basic Energy Sciences, for supporting the work done at Tufts University, under grant no. FG02-05ER15730, and the work done at the University of California, Davis, under grant no. FG02-04ER15513.

## LITERATURE CITED

1. Cornils B, Herrmann WA, eds. 2002. *Applied Homogeneous Catalysis with Organometallic Compounds*, Vol. 1. Weinhein: Wiley. 2nd ed.
2. Yermakov YI, Kuznetsov BN, Zakharov VA, eds. 1981. *Studies in Surface Science and Catalysis*, Vol. 8. Amsterdam: Elsevier
3. Ballard DGH. 1973. Pi and sigma transition metal carbon compounds as catalysts for the polymerization of vinyl monomers and olefins. *Adv. Catal.* 23:263–325
4. Basset JM, Gates BC, Candy JP, Choplin A, Leconte M, et al., eds. 1988. *Surface Organometallic Chemistry: Molecular Approaches to Surface Catalysis*, Vol. 231. New York: Springer
5. Hartley FR. 1985. *Supported Metal Complexes: A New Generation of Catalysts*. Boston: Reidel
6. Thomas JM, Saghi Z, Gai PL. 2011. Can a single atom serve as the active site in some heterogeneous catalysts? *Top. Catal.* 54:588–94

7. Gandhi HS, Graham GW, McCabe RW. 2003. Automotive exhaust catalysis. *J. Catal.* 216:433–42
8. Graham GW, Jen HW, Ezekoye O, Kudla RJ, Chun W, et al. 2007. Effect of alloy composition on dispersion stability catalytic activity for NO oxidation over alumina-supported Pt-Pd catalysts. *Catal. Lett.* 116:1–8
9. Adzic RR, Zhang J, Sasaki K, Vukmirovic MB, Shao M, et al. 2007. Platinum monolayer fuel cell electrocatalysts. *Top. Catal.* 46:249–62
10. Huber GW, Iborra S, Corma A. 2006. Synthesis of transportation fuels from biomass: chemistry, catalysis, and engineering. *Chem. Rev.* 106:4044–98
11. Skoplyak O, Barteau MA, Chen JG. 2008. Enhancing $H_2$ and CO production from glycerol using bimetallic surfaces. *ChemSusChem* 1:524–26
12. Thomas JM, Raja R. 2008. Exploiting nanospace for asymmetric catalysis: confinement of immobilzed, single-site chiral catalysts enhances enantioselectivity. *Acc. Chem. Res.* 41:708–20
13. Ratnasamy C, Wagner JP. 2009. Water gas shift catalysts. *Catal. Rev. Sci. Eng.* 51:325–440
14. Lu YC, Xu Z, Gasteiger HA, Chen S, Hamad-Schifferli K, Shao-Horn Y. 2010. Platinum-gold nanoparticles: a highly active bifunctional electrocatalyst for rechargeable lithium-air batteries. *J. Am. Chem. Soc.* 132:12170–71
15. Miessner H. 1994. Surface chemistry in a zeolite matrix: well-defined dinitrogen complexes of rhodium supported on dealuminated Y zeolite. *J. Am. Chem. Soc.* 116:11522–30
16. Miessner H, Richter K. 1998. Well-defined surface-bonded ruthenium complexes with molecular nitrogen. *Angew. Chem. Int. Ed. Engl.* 37:117–19
17. Landmesser H, Miessner H. 1991. Interaction of carbon monoxide with ruthenium supported on dealuminated Y zeolite. Evidence for the formation of a ruthenium tricarbonyl. *J. Phys. Chem.* 95:10544–46
18. Miessner H, Landmesser H, Jaeger N, Richter K. 1997. Surface carbonyl species of copper supported on dealuminated Y zeolite. *J. Chem. Soc. Faraday Trans.* 93:3417–22
19. Miessner H, Burkhardt I, Gutschick D, Zecchina A, Morterra C, Spoto G. 1989. The formation of well defined rhodium dicarbonyl in highly dealuminated rhodium-exchanged zeolite Y by interaction with CO. *J. Chem. Soc. Faraday Trans. 1* 85:2113–26
20. Fierro-Gonzalez JC, Kuba S, Hao Y, Gates BC. 2006. Oxide- and zeolite-supported molecular metal complexes and clusters: physical characterization and determination of structure, bonding, and metal oxidation state. *J. Phys. Chem. B* 110:13326–51
21. Guzman J, Gates BC. 2003. Supported molecular catalysts: metal complexes and clusters on oxides and zeolites. *Dalton Trans.* 2003:3303–18
22. Liang AJ, Craciun R, Chen M, Kelly TG, Kletnieks PW, et al. 2009. Zeolite-supported organorhodium fragments: essentially molecular surface chemistry elucidated with spectroscopy and theory. *J. Am. Chem. Soc.* 131:8460–73
23. Uzun A, Bhirud VA, Kletnieks PW, Haw JF, Gates BC. 2007. A site-isolated iridium diethylene complex supported on highly dealuminated Y zeolite: synthesis and characterization. *J. Phys. Chem. C* 111:15064–73
24. Ogino I, Gates BC. 2008. Molecular chemistry in a zeolite: genesis of a zeolite Y-supported ruthenium complex catalyst. *J. Am. Chem. Soc.* 130:13338–46
25. Guzman J, Gates BC. 2002. Simultaneous presence of cationic and reduced gold in functioning MgO-supported CO oxidation catalysts: evidence from x-ray absorption spectroscopy. *J. Phys. Chem. B* 106:7659–65
26. Aydin C, Lu J, Liang AJ, Chen C-Y, Browning ND, Gates BC. 2011. Tracking iridium atoms with electron microscopy: first steps of metal nanocluster formation in one-dimensional zeolite channels. *Nano Lett.* 11:5537–41
27. Ehresmann JO, Kletnieks PW, Liang A, Bhirud VA, Bagatchenko OP, et al. 2006. Evidence from NMR and EXAFS studies of a dynamically uniform mononuclear single-site zeolite-supported rhodium catalyst. *Angew. Chem. Int. Ed. Engl.* 45:574–76
28. Ogino I, Chen CY, Gates BC. 2010. Zeolite-supported metal complexes of rhodium and of ruthenium: a general synthesis method influenced by molecular sieving effects. *Dalton Trans.* 39:8423–31
29. Serna P, Gates BC. 2011. A bifunctional mechanism for ethene dimerization: catalysis by rhodium complexes on zeolite HY in the absence of halides. *Angew. Chem. Int. Ed. Engl.* 50:5528–31

30. Kletnieks PW, Liang AJ, Craciun R, Ehresmann JO, Marcus DM, et al. 2007. Molecular heterogeneous catalysis: a single-site zeolite-supported rhodium complex for acetylene cyclotrimerization. *Chem. Eur. J.* 13:7294–304
31. Ortalan V, Uzun A, Gates BC, Browning ND. 2010. Direct imaging of single metal atoms and clusters in the pores of dealuminated HY zeolite. *Nat. Nanotechnol.* 5:506–10
32. Uzun A, Gates BC. 2008. Real-time characterization of formation and breakup of iridium clusters in highly dealuminated zeolite Y. *Angew. Chem. Int. Ed. Engl.* 47:9245–48
33. Uzun A, Gates BC. 2009. Dynamic structural changes in molecular zeolite-supported iridium catalyst for ethene hydrogenation. *J. Am. Chem. Soc.* 131:15887–94
34. Vayssilov GN, Gates BC, Rösch N. 2003. Oxidation of supported rhodium clusters by support hydroxy groups. *Angew. Chem. Int. Ed. Engl.* 42:1391–94
35. Chang JR, Gron LU, Honji A, Sanchez KM, Gates BC. 1991. Mononuclear rhenium carbonyls on magnesia: characterization of the metal-support interface by extended x-ray fine structure spectroscopy. *J. Phys. Chem.* 95:9944–50
36. Fierro-Gonzalez JC, Gates BC. 2004. Mononuclear $Au^{III}$ and $Au^{I}$ complexes bonded to zeolite NaY: catalysts for CO oxidation at 298 K. *J. Phys. Chem. B* 108:16999–7002
37. Fierro-Gonzalez JC, Gates BC. 2005. Structural changes of gold-support interface during CO oxidation catalyzed by mononuclear gold complexes bonded to zeolite NaY: evidence from time-resolved X-ray absorption spectroscopy. *Langmuir* 21:5693–95
38. Lu J, Aydin C, Browning ND, Gates BC. 2012. Imaging gold atoms in site-isolated MgO-supported mononuclear gold complexes. *Angew. Chem.* In press
39. Tauster SJ, Fung SC, Garten RL. 1978. Strong-metal support interactions. Group 8 noble metals supported on titanium dioxide. *J. Am. Chem. Soc.* 100:170–75
40. Silvestre-Albero J, Sepúlveda-Escribano A, Rodríguez-Reinoso F, Anderson JA. 2004. Influence of Zn on the characteristics and catalytic behavior of $TiO_2$-supported Pt catalysts. *J. Catal.* 223:179–90
41. Nishihata Y, Mizuki J, Akao T, Tanaka H, Uenishi M, et al. 2002. Self-regeneration of a Pd-perovskite catalyst for automotive emissions control. *Nature* 418:164–67
42. Uenishi M, Tanigushi M, Tanaka H, Kimura M, Nishihata Y, et al. 2005. Redox behavior of palladium at start-up in perovskite-type $LaFePdO_x$ automotive catalysts showing a self-regeneration function. *Appl. Catal. B* 57:267–73
43. Shelef M, Graham GW, McCabe RW. 2002. Ceria and other oxygen storage components in automotive catalysts. See Ref. 51, pp. 343–75
44. Murrell LL, Tauster SJ, Anderson DR. 1991. Laser Raman characterization of surface phase precious metal oxides formed on $CeO_2$. *Studies Surf. Sci. Catal.* 71:275–89
45. Murrell LL, Tauster SJ, Anderson DR. 1993. Laser Raman characterization of surface phase precious metal oxides formed on $CeO_2$ micro domains generated within an alumina host by sol synthesis. *Studies Surf. Sci. Catal.* 75:681–90
46. Yoshida T, Sato A, Suzuki H, Tanabe T, Takahashi N. 2006. Development of high performance three-way catalyst. *SAE Paper No. 2006-01-0161.* doi: 10.4271/2006-01-1061
47. Hatanaka M, Takahashi N, Tanabe T, Nagai Y, Dohmae K, et al. 2010. Ideal Pt loading for a $Pt/CeO_2$-based catalyst stabilized by a Pt–O–Ce bond. *Appl. Catal. B* 99:336–42
48. Hatanaka M, Takahashi N, Takahashi N, Tanabe, T, Nagai Y, et al. 2009. Reversible changes in the Pt oxidation state and nanostructure on ceria-based supported Pt. *J. Catal.* 266:182–90
49. Shinjoh H, Hatanaka M, Nagai Y, Tanabe T, Takahashi N, et al. 2009. Suppression of noble metal sintering based on the support anchoring effect and its application in automotive three-way catalysis. *Top. Catal.* 52:1967–71
50. Sayle TXT, Parker SC, Sayle DC. 2005. Oxidising CO to $CO_2$ using ceria nanoparticles. *Phys. Chem. Chem. Phys.* 7:2936–41
51. Trovarelli A, ed. 2002. *Catalysis by Ceria and Related Materials*. London: Imperial Coll. Press
52. Liu W, Flytzani-Stephanopoulos M. 1995. Total oxidation of carbon monoxide and methane over transition metal-fluorite oxide composite metal catalysts: I. Catalyst composition and activity. *J. Catal.* 153:304–16

53. Liu W, Flytzani-Stephanopoulos M. 1995. Total oxidation of carbon monoxide and methane over transition metal-fluorite oxide composite metal catalysts: II. Catalyst characterization and kinetics. *J. Catal.* 153:317–32
54. Kundakovic LJ, Flytzani-Stephanopoulos M. 1998. Cu- and Ag-modified cerium oxide catalysts for methane oxidation. *J. Catal.* 179:203–21
55. Flytzani-Stephanopoulos M. 2001. Nanostructured cerium oxide ecocatalysts. *MRS Bull.* 26(11):885–89
56. Li Y, Fu G, Flytzani-Stephanopoulos M. 2000. Low-temperature water-gas shift reaction over Cu- and Ni-loaded cerium oxide catalysts. *Appl. Catal. B* 27:179–91
57. Fu Q, Saltsburg H, Flytzani-Stephanopoulos M. 2003. Active non-metallic Au and Pt species on ceria-based water-gas shift catalysts. *Science* 301:935–38
58. Bunluesin T, Putna ES, Gorte RJ. 1996. A comparison of CO oxidation on ceria-supported Pt, Pd, and Rh. *Catal. Lett.* 41:1–5
59. Bunluesin T, Gorte RJ, Graham GW. 1998. Studies of the water-gas shift reaction on ceria-supported Pt, Pd, and Rh: implications for oxygen-storage properties. *Appl. Catal. B* 15:107–14
60. Grabow LC, Gokhale AA, Evans ST, Dumesic JA, Mavrikakis M. 2008. Mechanism of the water gas shift reaction on Pt: first principles, experiments and microkinetic modeling. *J. Phys. Chem. C* 112:4608–17
61. Meunier FC, Goguet A, Hardacre C, Burch R, Thompsett D. 2007. Quantitative DRIFTS investigation of possible reaction mechanisms for the water-gas shift reaction on high-activity Pt- and Au-based catalysts. *J. Catal.* 252:18–22
62. Fu Q, Deng W, Saltsburg H, Flytzani-Stephanopoulos M. 2005. Activity and stability of low-content gold-ceria catalysts for the water-gas shift reaction. *Appl. Catal. B* 56:57–68
63. Qi X, Flytzani-Stephanopoulos M. 2004. Activity and stability of Cu-$CeO_2$ in high-temperature water-gas shift for fuel cell applications. *Ind. Eng. Chem. Res.* 43:3055–62
64. Si R, Raitano J, Yi N, Zhang L, Chan SW, Flytzani-Stephanopoulos M. 2012. Structure sensitivity of the low-temperature water-gas shift reaction on Cu-$CeO_2$ catalysts. *Catal. Today* 180:68–80
65. Hadjivanov KI, Vayssilov GN. 2002. Characterization of oxide surfaces and zeolites by carbon monoxide as an IR probe molecule. *Adv. Catal.* 47:307–511
66. Farrauto RJ, Hobson MC, Kennelly T, Waterman EM. 1992. Catalytic chemistry of supported palladium for combustion of methane. *Appl. Catal. A* 81:227–37
67. Colussi S, Trovarelli A, Vesselli E, Baraldi A, Comelli G, et al. 2010. Structure and morphology of $Pd/Al_2O_3$ and $Pd/CeO_2/Al_2O_3$ combustion catalysts in Pd-PdO transformation hysteresis. *Appl. Catal. A* 390:1–10
68. Ruckenstein E, Chen JJ. 1982. Wetting phenomena during alternating heating in $O_2$ and $H_2$ of supported metal crystallites. *J. Coll. Interf. Sci.* 86:1–11
69. McCabe RW, Usmen RK, Ober K, Gandhi HS. 1995. The effect of alumina phase structure on the dispersion of rhodium/alumina catalysts. *J. Catal.* 151:385–93
70. Ligthart DAJM, van Santen RA, Hensen EJM. 2011. Supported rhodium oxide nanoparticles as highly active CO oxidation catalysts. *Angew. Chem. Int. Ed. Engl.* 50:5306–10
71. Grass ME, Zhang Y, Butcher DR, Park JY, Li Y, et al. 2008. A reactive oxide overlayer on rhodium nanoparticles during CO oxidation and its size dependence studied by in situ ambient-pressure X-ray photoelectron spectroscopy. *Angew. Chem. Int. Ed. Engl.* 47:8893–96
72. Gustafson J, Westerstrom R, Resta A, Mikkelsen A, Andersen JN, et al. 2009. Structure and catalytic reactivity of Rh oxides. *Catal. Today* 145:227–35
73. Bera P, Gayen A, Hegde MS, Lalla NP, Spadaro L, et al. 2003. Promoting effect of $CeO_2$ in combustion synthesized $Pt/CeO_2$ for CO oxidation. *J. Phys. Chem. B* 107:6122–30
74. Pierre D, Deng W, Flytzani-Stephanopoulos M. 2007. The importance of strongly bound Pt-$CeO_x$ species for the water-gas shift reaction: catalytic stability and activity evaluation. *Top. Catal.* 46:363–73
75. Regalbuto J, ed. 2007. *Catalyst Preparation*. Boca Raton: CRC Press
76. Liu X, Korotkikh O, Farrauto R. 2002. Selective catalytic oxidation of CO in $H_2$: structural study of Fe oxide-promoted Pt/alumina catalysts. *Appl. Catal. A* 226:293–303
77. Wang X, Gorte RJ. 2003. The effect of Fe and other promoters on the activity of Pd/ceria for the water-gas shift reaction. *Appl. Catal. A* 247:157–62

78. Fu Q, Li WX, Yao YX, Liu HY, Su HY, et al. 2010. Interface-confined ferrous centers for catalytic oxidation. *Science* 328:1141–44
79. Ma T, Fu Q, Su HY, Liu HY, Cui Y, et al. 2009. Reversible structural modulation of Fe-Pt bimetallic surfaces and its effect on reactivity. *ChemPhysChem* 10:1013–16
80. Li S, Liu G, Lian H, Jia M, Zhao G, et al. 2008. Low-temperature CO oxidation over supported Pt catalysts prepared by colloid-deposition method. *Catal. Commun.* 9:1045–49
81. Liu L, Zhou F, Wang L, Qi X, Shi F, Deng Y. 2010. Low-temperature CO oxidation over Pt, Pd catalysts: particular $FeO_x$ support for oxygen supply during reactions. *J. Catal.* 274:1–10
82. Qiao B, Wang A, Yang X, Allard LF, Jiang Z, et al. 2011. Single-atom catalysis of CO oxidation using $Pt_1/FeO_x$. *Nat. Chem.* 3: 634–41
83. Sonström P, Arndt D, Wang X, Zielasek V, Bäumer M. 2011. Ligand capping of colloidally synthesized nanoparticles—a way to tune metal-support interactions in heterogeneous gas-phase catalysis. *Angew. Chem. Int. Ed. Engl.* 50:3888–91
84. Kwak JH, Hu JZ, Mei D, Yi CW, Kim DH, et al. 2009. Coordinatively unsaturated $Al^{3+}$ as centers for binding sites for active catalyst phases of platinum on $\gamma$-$Al_2O_3$. *Science* 325:1670–73
85. Zhai YP, Pierre D, Si R, Deng WL, Ferrin P, et al. 2010. Alkali-stabilized Pt-$OH_x$ species catalyze low-temperature water-gas shift reactions. *Science* 329:1633–36
86. Gokhale AA, Dumesic JA, Mavrikakis M. 2008. On the mechanism of low-temperature water-gas shift reaction on copper. *J. Am. Chem. Soc.* 130:1402–14
87. Yoshida H, Nonoyama S, Yazawa Y, Hattori T. 2010. Stabilization of high oxidation state platinum over basic support oxide examined by in situ laboratory XANES and temperature programmed desorption of oxygen. *Catal. Today* 153:156–61
88. Galvagno S, Parravano G. 1978. Chemical reactivity of supported gold: IV. Reduction of NO by $H_2$. *J. Catal.* 55:178–90
89. Bond GC, Sermon PA. 1973. Gold catalysts for olefin hydrogenation: transmutation of catalytic properties. *Gold Bull.* 6:102–5
90. Haruta M, Kobayashi T, Sano H, Yamada N. 1987. Novel gold catalysts for the oxidation of carbon monoxide at temperature far below 0°C. *Chem. Lett.* 2:405–8
91. Haruta M, Tsubota S, Kobayashi T, Kageyama H, Genet MJ, Delmon B. 1993. Low-temperature oxidation of CO over gold supported on $TiO_2$, $\alpha$-$Fe_2O_3$, and $Co_3O_4$. *J. Catal.* 144:175–92
92. Haruta M, Yamada N, Kobayashi T, Iijima S. 1989. Gold catalysts prepared by coprecipitation for low-temperature oxidation of hydrogen and carbon monoxide. *J. Catal.* 115:301–9
93. Nkosi B, Coville NJ, Hutchings GJ. 1988. Reactivation of a supported gold catalyst for acetylene hydrochlorination. *J. Chem. Soc. Chem. Commun.* 1988:71–72
94. Torres Sanchez RM, Ueda A, Tanaka K, Haruta M. 1997. Selective oxidation of CO in hydrogen over gold supported on manganese oxides. *J. Catal.* 168:125–27
95. Corma A, Concepción P, Serna P. 2007. A different reaction pathway for the reduction of aromatic nitro compounds on gold catalysts. *Angew. Chem. Int. Ed. Engl.* 46:7266–69
96. Alves L, Ballesteros B, Boronat M, Cabrero-Antonino JR, Concepción P, et al. 2011. Synthesis and stabilization of subnanometric gold oxide nanoparticles on multiwalled carbon nanotubes and their catalytic activity. *J. Am. Chem. Soc.* 133:10251–61
97. Hashmi ASK, Hutchings GJ. 2006. Gold catalysis. *Angew. Chem. Int. Ed. Engl.* 45:7896–936
98. Bond GC, Thompson DT. 1999. Catalysis by gold. *Catal. Rev. Sci. Eng.* 41:319–88
99. Bond GC, Louis C, Thompson DT. 2006. *Catalysis by Gold*. London: Imperial Coll. Press
100. Fierro-Gonzalez JC, Bhirud VA, Gates BC. 2005. A highly active catalyst for CO oxidation at 298 K: mononuclear $Au^{III}$ complexes anchored to $La_2O_3$ nanoparticles. *Chem. Commun.* 2005:5275–77
101. Valden M, Lai X, Goodman DW. 1998. Onset of catalytic activity of gold clusters on titania with the appearance of nonmetallic properties. *Science* 281:1647–50
102. Herzing AA, Kiely CJ, Carley AF, Landon P, Hutchings GJ. 2008. Identification of active gold nanoclusters on iron oxide supports for CO oxidation. *Science* 321:1331–35
103. Carrettin S, Concepción P, Corma A, López Nieto JM, Puntes VF. 2004. Nanocrystalline $CeO_2$ increases the activity of Au for CO oxidation by two orders of magnitude. *Angew. Chem. Int. Ed. Engl.* 43:2538–40

104. Guzman J, Carrettin S, Fierro-Gonzalez JC, Hao Y, Gates BC, Corma A. 2005. CO oxidation catalyzed by supported gold: Cooperation between gold and nanocrystalline rare-earth supports forms reactive surface superoxide and peroxide species. *Angew. Chem. Int. Ed. Engl.* 44:4778–81
105. Aguilar-Guerrero V, Lobo-Lapidus RJ, Gates BC. 2009. Genesis of a cerium oxide supported gold catalyst for CO oxidation: transformation of mononuclear gold complexes into clusters as characterized by X-ray absorption spectroscopy. *J. Phys. Chem. C* 113:3259–69
106. Lopez N, Janssens TVW, Clausen BS, Xu Y, Mavrikakis M, et al. 2004. On the origin of the catalytic activity of gold nanoparticles for low-temperature CO oxidation. *J. Catal.* 223:232–35
107. Fierro-Gonzalez JC, Gates BC. 2008. Catalysis by gold dispersed on supports: the importance of cationic gold. *Chem. Soc. Rev.* 37:2127–34
108. Kracke P, Haas T, Saltsburg H, Flytzani-Stephanopoulos M. 2010. CO oxidation on unsupported dendrimer-encapsulated gold nanoparticles. *J. Phys. Chem. C* 114:16401–7
109. Ketchie WC, Fang YL, Wong MS, Murayama M, Davis RJ. 2007. Influence of gold particle size on the aqueous-phase oxidation of carbon monoxide and glycerol. *J. Catal.* 250:94–101
110. Zhou Z, Flytzani-Stephanopoulos M, Kooi S, Saltsburg H. 2008. The role of the interface in CO oxidation on $Au/CeO_2$ multilayer nanotowers. *Advan. Funct. Mater.* 18:2801–7
111. Rodriguez JA, Ma S, Liu P, Hrbek J, Evans J, Pérez M. 2007. Activity of $CeO_x$ and $TiO_x$ nanoparticles grown on Au(111) in the water-gas shift reaction. *Science* 318:1757–60
112. Baron M, Bondarchuk O, Stacchiola D, Shaikhutdinov S, Freund HJ. 2009. Interaction of gold with cerium oxide supports: $CeO_2$(111) thin films versus $CeO_x$ nanoparticles. *J. Phys. Chem. C* 113:6042–49
113. Zhou Z, Saltsburg H, Flytzani-Stephanopoulos M. 2011. Decoration with ceria nanoparticles activates inert gold island/film surfaces for the CO oxidation reaction. *J. Catal.* 280:255–63
114. Lee Y, He G, Akey AJ, Si R, Flytzani-Stephanopoulos M, Herman IP. 2011. Raman analysis of mode softening in nanoparticle $CeO_{2-\delta}$ and Au-$CeO_{2-\delta}$ during CO oxidation. *J. Am. Chem. Soc.* 133:12952–55
115. Green IX, Tang W, Neurock M, Yates JT. 2011. Spectroscopic observation of dual catalytic sites during oxidation of CO on a $Au/TiO_2$ catalyst. *Science* 333:736–39
116. Fugitani T, Nakamura I. 2011. Mechanism and active sites of the oxidation of CO over $Au/TiO_2$. *Angew. Chem. Int. Ed. Engl.* 50:10144–47
117. Lee S, Molina LM, Lopez MJ, Alonso JA, Hammer B, et al. 2009. Selective propene epoxidation on immobilized $Au_{6-10}$ clusters: the effect of hydrogen and water on activity and selectivity. *Angew. Chem. Int. Ed. Engl.* 48:1467–71
118. Huang J, Akita T, Faye J, Fujitani T, Takei T, Haruta M. 2009. Propene epoxidation with dioxygen catalyzed by gold clusters. *Angew. Chem. Int. Ed. Engl.* 48:7862–66
119. Date M, Okumura M, Tsubota S, Haruta M. 2004. Vital role of moisture in the catalytic activity of supported gold nanoparticles. *Angew. Chem. Int. Ed. Engl.* 43:2129–32
120. Kung HH, Kung MC, Costello CK. 2003. Supported Au catalysts for low temperature CO oxidation. *J. Catal.* 216:425–32
121. Gao F, Wood TE, Goodman DW. 2010. The effects of water on CO oxidation over $TiO_2$ supported Au catalysts. *Catal. Lett.* 134:9–12
122. Kim WB, Voitl T, Rodriguez-Rivera GJ, Dumesic JA. 2004. Powering fuel cells with CO via aqueous polyoxometalates and gold catalysts. *Science* 305:1280–83
123. Zope BN, Hibbitts DD, Neurock M, Davis RJ. 2010. Reactivity of the gold/water interface during selective oxidation catalysis. *Science* 330:74–78
124. Veith GM, Lupini AR, Dudney NJ. 2008. Role of pH in the formation of structurally stable and catalytically active $TiO_2$-supported gold catalysts. *J. Phys. Chem. C* 113:269–80
125. Veith GM, Lupini AR, Pennycook SJ, Dudney NJ. 2010. Influence of support hydroxides on the catalytic activity of oxidized gold clusters. *ChemCatChem* 2:281–86
126. Takei T, Okuda I, Bando KK, Akita T, Haruta M. 2010. Gold clusters supported on $La(OH)_3$ for CO oxidation at 193 K. *Chem. Phys. Lett.* 493:207–11
127. Gluhoi AC, Nieuwenhuys BE. 2007. Structural and chemical promoter effects of alkali (earth) and cerium oxides in CO oxidation on supported gold. *Catal. Today* 122:226–32

128. Mihaylov M, Ivanova E, Hao Y, Hadjiivanov K, Knözinger H, Gates BC. 2008. Gold supported on $La_2O_3$: structure and reactivity with $CO_2$ and implications for CO oxidation catalysis. *J. Phys. Chem. C* 112:18973–83
129. Andreeva D, Idakiev V, Tabakova T, Andreev A. 1996. Low-temperature water-gas shift reaction over Au/$\alpha$-$Fe_2O_3$. *J. Catal.* 158:354–55
130. Fu Q, Weber A, Flytzani-Stephanopoulos M. 2001. Nanostructured Au-$CeO_2$ catalysts for low-temperature water-gas shift. *Catal. Lett.* 77:87–95
131. Boccuzzi F, Chiorino A, Manzoli M, Andreeva D, Tabakova T. 1999. FTIR study of the low-temperature water-gas shift reaction on Au/$Fe_2O_3$ and Au/$TiO_2$ catalysts. *J. Catal.* 188:176–85
132. Fu Q, Kudriavtseva S, Saltsburg H, Flytzani-Stephanopoulos M. 2003. Gold-ceria catalysts for low-temperature water-gas shift reaction. *Chem. Eng. J.* 93:41–53
133. Liu ZP, Jenkins SJ, King DA. 2005. Origin and activity of oxidized gold in water-gas-shift catalysis. *Phys. Rev. Lett.* 94:196102
134. Deng W, Frenkel AI, Si R, Flytzani-Stephanopoulos M. 2008. Reaction-relevant gold structures in the low temperature water-gas shift reaction on Au-$CeO_2$. *J. Phys. Chem. C* 112:12834–40
135. Castellani NJ, Branda MM, Neyman KM, Illas F. 2009. Density functional theory study of the adsorption of Au atom on cerium oxide: effect of low-coordinated surface sites. *J. Phys. Chem. C* 113:4948–54
136. Tabakova T, Boccuzzi F, Manzoli M, Sobczak JW, Idakiev V, Andreeva D. 2006. A comparative study of nanosized IB/ceria catalysts for low-temperature water-gas shift reaction. *Appl. Catal. A* 298:127–43
137. Tibiletti D, Fonseca AA, Burch R, Chen Y, Fisher JM, et al. 2005. DFT and in situ EXAFS investigation of gold/ceria-zirconia low-temperature water gas shift catalysts: identification of the nature of the active form of gold. *J. Phys. Chem. B* 109:22553–59
138. Wang X, Rodriguez JA, Hanson JC, Perez M, Evans J. 2005. In situ time-resolved characterization of Au-$CeO_2$ and $AuO_x$-$CeO_2$ catalysts during the water-gas shift reaction: presence of Au and O vacancies in the active phase. *J. Chem. Phys.* 123:221101
139. Deng W, Flytzani-Stephanopoulos M. 2006. On the issue of the deactivation of Au–ceria and Pt–ceria water-gas shift catalysts in practical fuel-cell applications. *Angew. Chem. Int. Ed. Engl.* 45:2285–89
140. Deng W, Carpenter C, Yi N, Flytzani-Stephanopoulos M. 2007. Comparison of the activity of Au/$CeO_2$ and Au/$Fe_2O_3$ catalysts for the CO oxidation and the water-gas shift reactions. *Top. Catal.* 44:199–208
141. Si R, Flytzani-Stephanopoulos M. 2008. Shape and crystal-plane effects of nanoscale ceria on the activity of Au-$CeO_2$ catalysts for the water-gas shift reaction. *Angew. Chem. Int. Ed. Engl.* 47:2884–87
142. Boucher MB, Goergen S, Yi N, Flytzani-Stephanopoulos M. 2011. "Shape effects" in metal oxide supported nanoscale gold catalysts. *Phys. Chem. Chem. Phys.* 13:2517–27
143. Yi N, Si R, Saltsburg H, Flytzani-Stephanopoulos M. 2010. Steam reforming of methanol over ceria and gold-ceria nanoshapes. *Appl. Catal. B* 95:87–92
144. Yi N, Si R, Saltsburg H, Flytzani-Stephanopoulos M. 2010. Active gold species on cerium oxide nanoshapes for methanol steam reforming and the water gas shift reactions. *Energy Environ. Sci.* 3:831–37
145. Boucher MB, Yi N, Gittleson F, Zugic B, Saltsburg H, Flytzani-Stephanopoulos M. 2011. Hydrogen production from methanol over gold supported on ZnO and $CeO_2$ nanoshapes. *J. Phys. Chem. C* 115:1261–68
146. Allard LF, Borisevich A, Deng W, Si R, Flytzani-Stephanopoulos M, Overbury SH. 2009. Evolution of gold structure during thermal treatment of Au/$FeO_x$ catalysts revealed by aberration-corrected electron microscopy. *J. Electron Microsc.* 58:199–212
147. Allard LF, Flytzani-Stephanopoulos M, Overbury SH. 2010. Behavior of Au species in Au/$Fe_2O_3$ catalysts characterized by novel in situ heating techniques and aberration-corrected STEM imaging. *Microsc. Microanal.* 16(4):375–85
148. Rim KT, Eom D, Liu L, Stolyarova E, Raitano JM, et al. 2009. Charging and chemical reactivity of gold nanoparticles and adatoms on the (111) surface of single-crystal magnetite: a scanning tunneling microscopy/spectroscopy study. *J. Phys. Chem. C* 113(23):10198–205
149. Williams WD, Shekhar M, Lee W-S, Kispersky V, Delgass WN, et al. 2010. Metallic corner atoms in gold clusters supported on rutile are the dominant active site during water–gas shift catalysis. *J. Am. Chem. Soc.* 132:14018–20

150. Guzman J, Gates BC. 2003. Structure and reactivity of a mononuclear gold-complex catalyst supported on magnesium oxide. *Angew. Chem. Int. Ed. Engl.* 42(6):690–93
151. Guzman J, Gates BC. 2004. A mononuclear gold complex catalyst supported on MgO: spectroscopic characterization during ethylene hydrogenation catalysis. *J. Catal.* 226:111–19
152. Uzun A, Ortalan V, Hao Y, Browning ND, Gates BC. 2009, Imaging gold atoms in site-isolated MgO-supported mononuclear gold complexes. *J. Phys. Chem. C* 113:16847–49

Annual Review of Chemical and Biomolecular Engineering

Volume 3, 2012

# Contents

**Indexes**



**Errata**

An online log of corrections to *Annual Review of Chemical and Biomolecular Engineering* articles may be found at http://chembioeng.annualreviews.org/errata.shtml